

A surprisingly high number of dual active galactic nuclei in the early Universe

Michele Perna^{1*}, Santiago Arribas¹, Isabella Lamperti¹,
 Chiara Circosta^{2,3}, Elena Bertola⁴, Pablo G. Pérez-González¹,
 Francesco D'Eugenio^{5,6}, Hannah Übler^{5,6}, Giovanni Cresci³,
 Roberto Maiolino^{5,6,3}, Bruno Rodríguez Del Pino¹,
 Andrew J. Bunker⁷, Stéphane Charlot⁸, Chris J. Willott⁹,
 Stefano Carniani¹⁰, Torsten Böker¹¹, Jacopo Chevallard³,
 Mirko Curti¹², Gareth Jones⁷, Nimisha Kumari¹¹,
 Madeline A. Marshall^{9,13}, Aayush Saxena⁷, Jan Scholtz^{5,6},
 Giacomo Venturi¹⁰, Joris Witstok^{5,6}

¹Centro de Astrobiología (CAB), CSIC-INTA, Departamento de Astrofísica, Cra. de Ajalvir Km. 4, 28850 – Torrejón de Ardoz, Madrid, Spain.

²European Space Agency, ESAC, Villanueva de la Cañada, E-28692 Madrid, Spain.

³Department of Physics and Astronomy, University College London, Gower Street, London WC1E 6BT, UK.

⁴INAF - Osservatorio Astrofisico di Arcetri, largo E. Fermi 5, 50127 Firenze, Italy.

⁵Kavli Institute for Cosmology, University of Cambridge, Madingley Road, Cambridge, CB3 0HA, UK.

⁶Cavendish Laboratory - Astrophysics Group, University of Cambridge, 19 JJ Thomson Avenue, Cambridge, CB3 0HE, UK.

⁷University of Oxford, Department of Physics, Denys Wilkinson Building, Keble Road, Oxford OX13RH, United Kingdom.

⁸Sorbonne Université, UPMC-CNRS, UMR7095, Institut d'Astrophysique de Paris, F-75014 Paris, France.

⁹NRC Herzberg, 5071 West Saanich Rd, Victoria, BC V9E 2E7, Canada.

¹⁰Scuola Normale Superiore, Piazza dei Cavalieri 7, I-56126 Pisa, Italy.

¹¹European Space Agency, c/o STScI, 3700 San Martin Drive, Baltimore, MD 21218, USA.

¹²European Southern Observatory, Karl-Schwarzschild-Strasse 2, 85748
Garching, Germany.

¹³ARC Centre of Excellence for All Sky Astrophysics in 3 Dimensions
(ASTRO 3D), Australia.

*Corresponding author(s). E-mail(s): michele.perna@cab.inta-csic.es;

Merger events can trigger gas accretion onto supermassive black holes (SMBHs) sitting at the centre of galaxies, and form close pairs of active galactic nuclei (AGN)¹. The fraction of AGN in pairs gives key information to constrain the environmental properties and evolution of SMBHs and their host galaxies^{2–5}. However, the identification of dual AGN is difficult, and only very few have been found in the distant Universe so far^{6–8}.

We report the serendipitous discovery of a triple AGN and four dual AGN (one considered as a candidate), with projected separations in the range 3–28 kiloparsecs. Their AGN classification is mostly based on classical optical emission line flux ratios⁹, as observed with the Near-Infrared Spectrograph (NIRSpec) on the James Webb Space Telescope (JWST), and is complemented with additional multi-wavelength diagnostics^{10, 11}.

The identification of these multiple AGN out of the 17 AGN systems in our GA-NIFS^{12, 13} survey (i.e. $\sim 20\text{--}30\%$), suggests that they might be more common than expected from the most recent cosmological simulations, which predict a fraction of dual AGN at least one order of magnitude smaller^{3, 4}. This work highlights the exceptional capabilities of NIRSpec for detecting distant dual AGN, and prompts new investigations to better constrain their fraction across the cosmic time, and to inform upcoming cosmological simulations.

Since SMBHs are believed to be present at the centre of most massive galaxies (e.g. [14]), merging systems with two or more SMBHs are a natural and expected occurrence ([15]). Their study has received increasing attention, as they can be used to constrain the link between galaxy mergers and SMBH feeding and feedback effects across cosmic time, a key ingredient for galaxy evolution models ([3–5]). However, systems with multiple SMBHs in the distant Universe can only be revealed during short-lived phases of galaxy mergers, when gas and dust fall into their deep gravitational wells, and their nuclei shine as AGN (e.g. [2]). Cosmological simulations predict a fraction of AGN pairs - separated by hundreds to tens of thousands parsecs - out of the total number of AGN, of the order of a few percent in the redshift range $1 < z < 5$ (e.g. [3–5]). Observations have been consistent to date with these theoretical predictions: so far, only very few dual AGN have been found at $z > 1$ (e.g. [6–8]).

Many dual AGN have been discovered serendipitously (e.g. [16, 17]), because of the inherent difficulty in identifying these systems ([3]). However, more recently, systematic searches have started thanks to the development of new techniques taking full advantage of the all-sky Gaia database ([18]). The Gaia-Multi-Peak (GMP [7]) technique allows for the identification of dual AGN candidates at separations in the range 0.1-0.7'' (e.g. 0.8–5.5 kpc at $z = 3$), looking for multiple peaks in the radial light profile of bright sources. Another method is the Varstrometry technique ([19]), which extends systematic searches for dual AGN candidates at separations down to milli-arcsecond scales (e.g. < 50 pc at $z = 3$) exploiting the temporal displacements of the photocenter of unresolved sources.

These new methods have proven to be effective in discovering new dual AGN (up to $z \sim 3$ [6, 8]). However, they still require dedicated follow-up strategies to spatially and spectrally resolve the candidate AGN pairs as well as to distinguish multiple spatial components due to gravitational lensing of a single active galaxy from real AGN pairs ([6]). These methods have also an important observational bias, as require that these systems must significantly emit in the optical band ($\sim 4000 - 9500 \text{ \AA}$) in order to be selected with Gaia. As a consequence, all dual AGN discovered with Gaia are unlikely to be heavily affected by dust extinction. This is an important limitation, since an enhanced level of AGN obscuration is actually expected in late-stage mergers (e.g. [20–23]).

JWST, with its orders of magnitude improvement in sensitivity and resolution across the wavelength range from 0.6 to 28.8 μm compared to the previous generation of infrared telescopes [24], is showing us our Universe in a whole new light. Namely, it is opening the opportunity to study in detail the environment of AGN in the early Universe, by probing their emission in the rest-frame ultraviolet (UV) and optical spectral ranges. The first few JWST spatially resolved spectroscopic observations obtained with the integral field spectrograph (IFS) of NIRSpec ([25, 26]) and the wide field slitless spectroscopy (WFSS) mode of NIRCам ([27]) have already revealed that high- z AGN are often surrounded by close companions ([12, 13, 28–30]). Moreover, JWST observations show tidal bridges and tails at kiloparsec scales connecting the AGN with the companions, hence revealing the presence of gravitational interactions up to $z \sim 7$ (e.g. [28]). These data also allow to unveil the nature of the AGN companions: for instance, classical emission line flux ratio diagnostics such as the optical and UV diagrams (e.g. [9–11]) can be used to identify multiple AGN.

In this work we report the discovery of a triple AGN, three confirmed and a candidate dual AGN at $z \sim 3.5$, as listed in Table 1. They have projected separations between 3 and 28 kpc, and are located in the GOODS-S ([31]) and COSMOS fields ([32]); this work, therefore, doubles the number of known multiple AGN systems at $z > 3$ with separations < 30 kpc ([8]). All AGN pairs have been observed with NIRSpec IFS; the triple AGN has been instead identified by combining NIRSpec and archival observations from the optical IFS Multi Unit Spectroscopic Explorer (MUSE) at the Very Large Telescope (VLT). The sample of multiple AGN systems was created from a larger sample of 17 AGN systems at $2 < z < 6$, with bolometric luminosities in the range $L_{bol} \approx 10^{44} - 10^{46} \text{ erg s}^{-1}$, targeted as part of the JWST

program *Galaxy Assembly with NIRSpect IFS* (GA-NIFS). Of those, 13 sources were selected solely for their (absorption-corrected) X-ray luminosity, $L_{2-10 \text{ keV}} \gtrsim 10^{44} \text{ erg s}^{-1}$, unambiguously associated with nuclear emission; four sources initially classified as non-active star-forming (SF) galaxies were added to the active galaxies sample, as they show AGN features in their optical spectra (see Methods).

The identification of the dual AGN was made possible thanks to the detection of bright $[\text{O III}]\lambda 5007$ ($[\text{O III}]$ hereinafter) emitters in the surroundings of the primary AGN, placed at the centre of the NIRSpect IFS field-of-view ($3'' \times 3''$). These sources are displayed in Fig. 1, and are labeled as AGN-A, indicating the primary (brighter) nucleus, and AGN-B, indicating the secondary (fainter) nucleus. They are classified as AGN on the basis of the standard optical diagnostic diagram known as BPT ([9], see Fig. 2a), which is commonly used to identify the ionising mechanism of emitting gas. Although the separation between active and non-active galaxies in the BPT at $z \gtrsim 3$ is not yet well established (it was not possible to measure the lines required for the BPT at such redshifts before the advent of JWST), we note that the flux ratios of our AGN are higher than those of the distant SF galaxies so far observed (e.g. [33–35]); moreover, SF ionisation model predictions (e.g. [10, 11]) cannot reproduce our measurements. In some cases, we complemented BPT-based AGN classification with the presence of particularly prominent $[\text{O III}]$ outflows (with velocities of several hundred km s^{-1}), Balmer line broad-line-region (BLR), and X-ray emission in the AGN pairs, all unambiguously associated with accreting SMBHs.

The identification of the triple AGN relies on rest-frame optical NIRSpect observations, for what concerns the primary and secondary AGN (Figs. 1e, 2a). Additional analysis of archival MUSE observations (Fig. 3) allowed us to identify a third AGN $\sim 3.6''$ south-west of the primary nucleus, through its UV spectrum: it shows strong AGN emission lines, according to the UV diagnostics presented by, for instance, [10] (Fig. 2b), and [11].

Further emission-line diagnostics ([36]) confirmed that the ionising luminosity coming from the primary AGN is not sufficient to explain the luminosity of the secondary (and tertiary) sources in our multiple AGN systems. Intrinsic AGN ionisation is required for all but the GS551-B source (see Methods): we found that the lower limit on the incident ionising luminosity on GS551-B (produced by the primary AGN) is just a factor of 4 higher than the luminosity required to explain its line emission (much higher values are instead found for all other AGN companions). Considering the uncertainties associated to the computation, we conclude that this factor of 4 is not enough to firmly classify this system as an AGN pair. Therefore, GS551-A and B are considered as a dual AGN candidate.

For most of the newly discovered AGN, we were able to measure their stellar masses, $M_* \approx 10^8 - 10^{11} M_\odot$, depending on the availability of multi-wavelength information (see Table 1, and Methods). Therefore, we can confirm that (most of) these companions are not low-mass satellites and can be actually related to ongoing major merger events. The best confirmation of this scenario is represented by COS1638 (Fig. 1a), also showing two distinct dust emitters at the position of the sources (AGN-B is

brighter than the primary AGN host at ~ 1 mm, see Extended Data B)). In Table 1 we report the spectroscopic redshifts, coordinates, stellar masses and bolometric luminosities for our newly discovered multiple AGN systems, together with the criteria used to identify the AGN; each system is described in detail in Extended Data B.

Taking as a reference the predicted AGN fractions obtained from different cosmological simulations and homogenised by [3], one would expect a fraction of 1–5% dual AGN at projected separations < 30 kpc and with luminosities $L_{bol} > 10^{43}$ erg s $^{-1}$ (see also [4, 5]). In spite of the small size of the GA-NIFS sample (17 AGN systems), our findings are definitely at odds with such predictions, pointing to the presence of a much larger population of dual AGN in the early Universe, up to ~ 20 –30% of the total number of active galaxies (see also [37]). Interestingly, our results are more in line with a different outcome of the simulations mentioned above: they predict fractions of SMBH pairs in which only one nucleus is active (hence identified as AGN) of the order of 10–20% at $z \sim 3$ (see Fig. 6 in [3]). It is therefore possible that part of the inconsistency between our observations and the dual AGN predictions resides in the fact that assessing in simulations whether a SMBH is accreting or not, at the time of observation, is regulated by assumptions at the sub-grid physics level ([3, 37]). However, idealised merger simulations able to follow the dynamics of SMBHs at sub-kpc scales (hence avoiding the assumptions required in cosmological simulations), are similarly pointing to very small dual AGN fractions: [38] found that most of the AGN activity during the mergers is non-simultaneous, resulting in an expected fraction of dual AGN of 4–5% (see also [2]).

Future JWST spectroscopic surveys will be used to better constrain the fraction of dual AGN in the early Universe; these observations will inform upcoming cosmological and high-resolution hydrodynamical simulations, and also guide the comparison with gravitational wave experiments (e.g. [39]).

Figures and tables

Table 1: Dual (and triple) AGN

target	redshift	RA & DEC (degrees)	Separation ($''$) (kpc)		$\log(M_*)$ (M_\odot)	$\log(L_{\text{bol}})$ (erg s^{-1})	C_{AGN}
(1)	(2)	(3)	(4)	(5)	(6)	(7)	(8)
COS1638-A	3.5079	150.735557 +2.19953	–	–	$10.9 \pm 0.4^\dagger$	46.7	2,3,4
COS1638-B	3.5109	150.735847 +2.19962	1.1	8.2	$11.1 \pm 0.4^\dagger$	46.2	1,2,4 [‡]
GS551-A	3.7026	53.124385 –27.85169	–	–	10.9 ± 0.3	46.0	1,2,4*,5
GS551-B ¹	3.7022	53.124274 –27.85166	0.4	2.9	–	44.5	1
Enfield (AGN-A)	3.7149	150.061668 +2.37887	–	–	9.5 ± 0.2	44.8	1,2 [‡]
Mr. West (AGN-B)	3.7096	150.061348 +2.37877	1.2	8.8	9.4 ± 0.3	44.3	1,2 [‡]
COS1656-A	3.5101	150.271546 +1.61383	–	–	11.0 ± 0.2	45.8	1,2,4
COS1656-B	3.5092	150.271589 +1.61424	1.4	10.4	9.7 ± 0.3	44.3	1
GS10578-A	3.0647	53.165325 –27.81415	–	–	11.2 ± 0.2	44.6	1,2,4,5
GS10578-B	3.0643	53.165532 –27.81415	0.7	4.7	–	44.2	1
LAE2	3.0674	53.164688 –27.81489	3.6	28	8.3 ± 0.4	$\lesssim 44.6$	5

Column (1): target name. Enfield and Mr. West identify the newly discovered companion of Jekyll & Hyde, following Pérez-González et al., in prep. Column (2): Redshift, as measured from the narrower Gaussian component in the UV and optical spectra (typical uncertainty of 0.0002). Column (3): Coordinates RA & DEC. Columns (4) and (5): separation of the secondary (and tertiary) AGN from the primary nucleus. Column (6): stellar mass, as inferred from spectral energy distribution analysis (see Methods); for COS1638-A and its close companion we provided order of magnitude estimates assuming a conservative M_{dust}/M_* (see Methods). Column (7): bolometric luminosity, measured from the NLR $H\beta$ flux using Eq. 3 of [45] (typical uncertainty of 0.1 dex, not taking into account the bolometric correction scatter), for all but the AGN in LAE2 for which UV continuum is instead used (see Methods). Column (8): flags on specific criteria used to identify AGN: 1= BPT diagram, 2= prominent [O III] outflow, 3= BLR emission, 4= X-ray emission, 5= UV line ratios of [10] and [11].

¹Candidate secondary AGN, as incident ionizing flux from the primary AGN could be responsible for the observed fluxes in AGN-B, see Methods.

[†]: tentative estimate, see Methods.

[‡]: tentative evidence, see Methods.

*: X-ray emission likely associated with both sources.

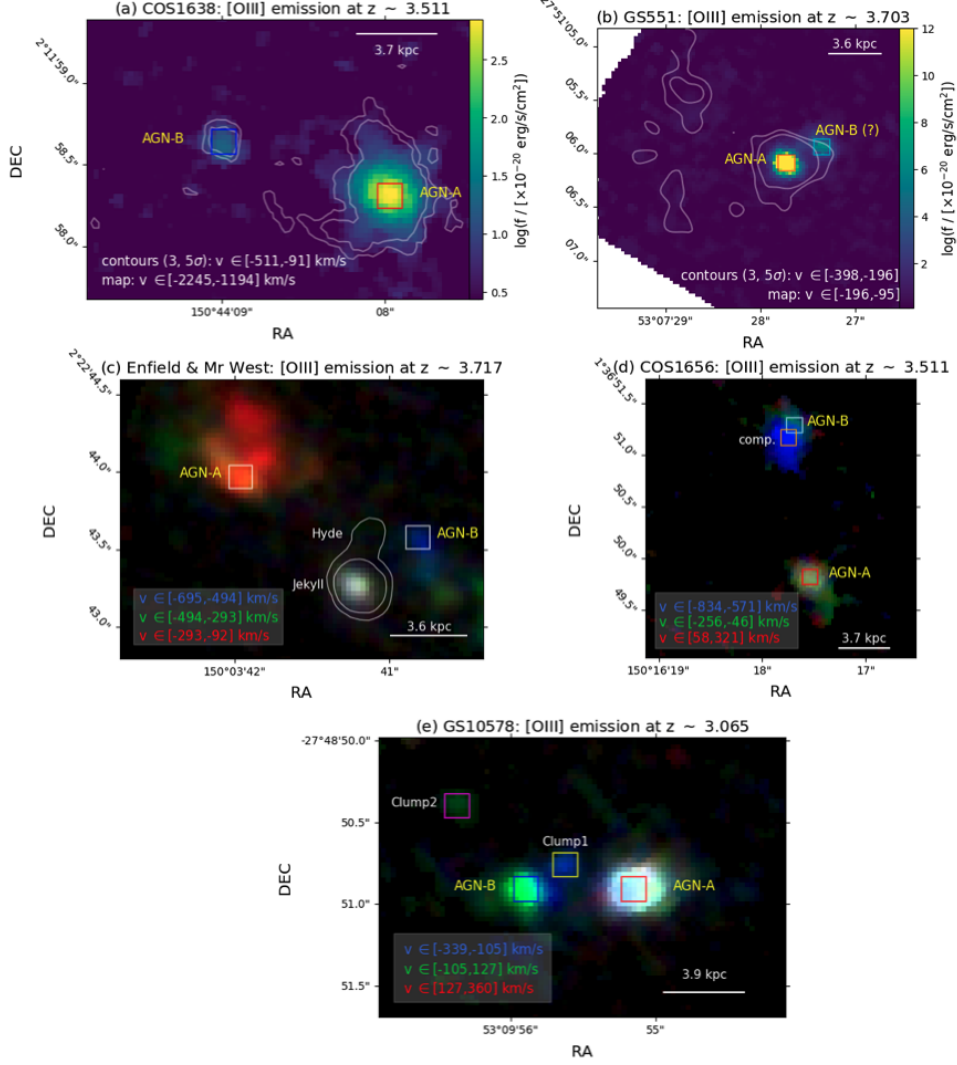


Fig. 1: [O III] maps and false-colour images of the multiple AGN systems: they are obtained by integrating the [O III] emission over specific velocity ranges (as labeled), in order to highlight the primary (AGN-A) and secondary (AGN-B) nuclei, together with additional structures at the same redshift of the active galaxies. The contours in panels *a* and *b* display filamentary structures possibly due to ongoing mergers, traced by [O III] gas at a few hundred km s^{-1} . The contours in panel *c* trace the Jekyll & Hyde continuum emission at $\sim 1\mu\text{m}$ (rest-frame), as observed with NIRSpc; the companions Enfield and Mr. West (AGN-A and B in panel *c*) are identified here for the first time. The system shown in panel *e* also comprises an AGN-C, outside of the NIRSpc field-of-view (see Fig. 3). All velocity ranges used to generate these images (reported in each panel) are also represented in the spectra in Fig. A1, extracted from the box regions labeled in the [O III] maps.

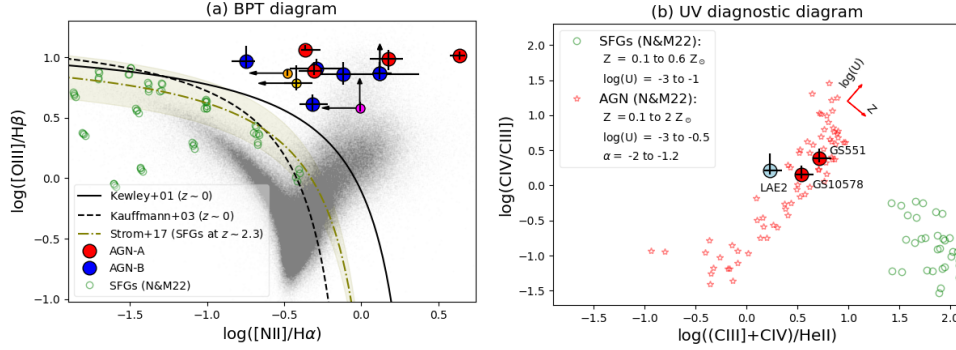


Fig. 2: (a) BPT diagram: Large red and blue circles refer to primary (AGN-A) and secondary (AGN-B) nuclei, respectively; small filled circles identify additional [O III] emitters in the vicinity of the active galaxies (with colors matching the boxes in Fig. 1). All AGN are above the solid ([40]) and dashed ([41]) curves, used to separate purely SF galaxies (below the curves) from galaxies containing AGN (above) in the local Universe. For the remaining targets (smaller filled symbols) we cannot discriminate between AGN and SF ionisation, because of the upper limits on $[\text{N II}]/\text{H}\alpha$. In the figure, we also report a olive curve indicating the locus of $z \sim 2.3$ SF galaxies from [42] (with intrinsic scatter relative to the median curve in light-olive), small grey points representing SF galaxies and AGN from SDSS [43], and small green symbols indicating model predictions for SF galaxies from [10] (see legend in panel b). **(b) UV diagnostic diagram:** Small green and red symbols represent model predictions for SF galaxies and AGN, respectively, from [10] (see legend for details about model parameters). Larger symbols refer to the MUSE measurements of the three AGN in our sample, as labeled: these sources occupy the AGN region of the diagram, with relatively high metallicity ($Z \approx 1 Z_{\odot}$) and hard ionising spectrum (ionization parameter $\log(U) \gtrsim -2$; see the orthogonal red arrows in the figure).

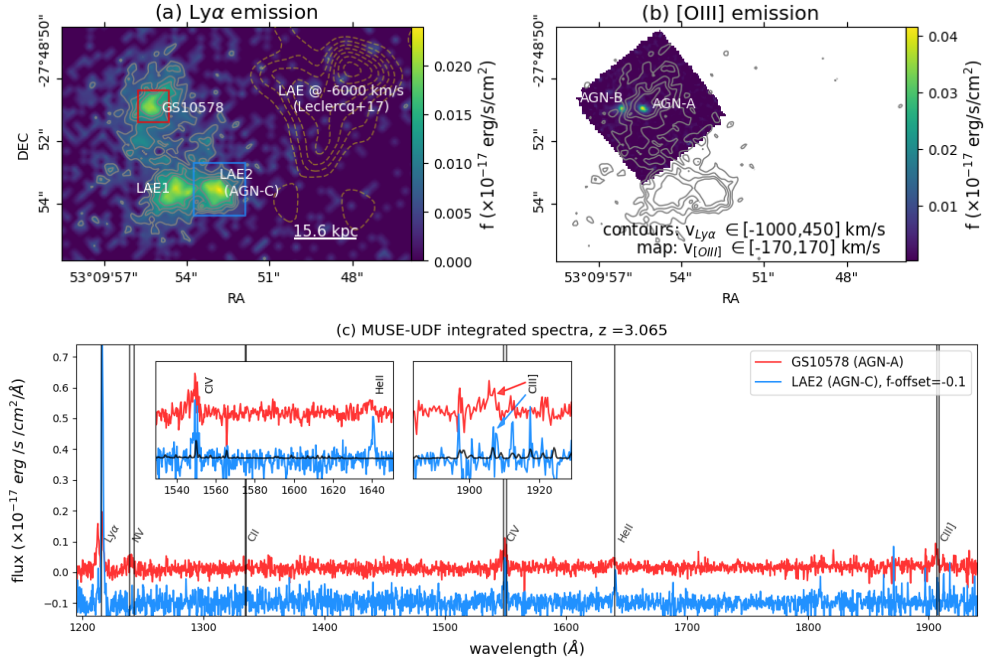


Fig. 3: (a & b) Triple AGN emission line maps: GS10578 Ly α (*left*) and [O III] (*right*) maps obtained from MUSE and NIRSspec data cubes, respectively; the Ly α image was re-gridded to match the size of the NIRSspec spaxels. The Ly α map and grey contours trace the Ly α emitting gas within $v \in [-1000, +450]$ km s $^{-1}$ from the systemic velocity of GS10578, and show two additional emitters, labeled LAE1 and LAE2. The orange contours indicate the Ly α emission of a nearby source identified by [44]. The [O III] map shows the two point-like sources already identified in Fig. 1e. **(c) UV spectra of the triple AGN:** MUSE spectra of GS10578 (red) and LAE2 (lightblue), showing strong AGN emission lines, according to UV diagnostics (Fig. 2b). These spectra have been extracted from the boxes indicated in the top-left map, and reported in the rest-frame; for visual purposes, the LAE2 spectrum has been shifted, as labeled. The zoom-in insets show the same spectra in the vicinity of the lines used in the UV diagnostics, together with 1 σ errors for the LAE2 spectrum (black curve, mostly highlighting the position of strong sky line residuals). No other emission lines are detected in the LAE1 spectrum (apart from Ly α).

Methods

Cosmological model

The cosmological parameters adopted in this paper are $H_0 = 70 \text{ km s}^{-1} \text{ Mpc}^{-1}$, $\Omega_m = 0.3$, and $\Omega_\Lambda = 0.7$.

Sample

“Galaxy Assembly with NIRSpect IFS” (GA-NIFS) is a JWST Guaranteed Time Observations (GTO) program which aims to characterise the internal structure and close environment of a sample of high- z ($z > 2$) galaxies, and to investigate the physical processes driving galaxy evolution across cosmic time ([12, 13, 28, 46–50]). It comprises 55 targets to be observed with NIRSpect IFS in JWST cycles 1 and 3, including both SF galaxies and AGN.

The sub-sample of non-active galaxies has been heterogeneously selected among the most luminous and/or extended sources (as observed in $\text{Ly}\alpha$, NIR, and/or mm wavelengths), together with a few well studied sources (e.g. Jekyll & Hyde [51]), to increase the leverage of IFS capabilities.

The sub-sample of active galaxies includes sources at $z < 6$ residing in the COSMOS and GOODS-S fields, and selected solely for their X-ray emission, which is unambiguously attributed to AGN emission ($L_{2-10 \text{ keV}} \gtrsim 10^{44} \text{ erg s}^{-1}$ [52, 53]). This sub-sample consists of 7 sources in GOODS-S and 6 in COSMOS. A careful inspection of the NIRSpect data of other GA-NIFS targets in the same cosmological fields - but not fitting in the above X-ray selection criterion - allowed us to identify additional targets: we unveiled the presence of AGN activity, based on BPT diagnostics, in (the vicinity of) three sources originally selected as non-active galaxies, GS19293 (Circosta et al., in prep.), Jekyll (Pérez-González et al., in prep.), and HZ10 (Cresci et al., in prep.). GS3073 must also be considered an AGN, because of the detection of BLR emission in its rest-frame optical spectrum ([12]). Therefore, the sub-sample of AGN used in this work comprises 17 systems at $2.0 < z < 5.7$ (see Table A1), with ($H\beta$ -based) bolometric luminosities in the range $L_{bol} = 10^{44} - 10^{46} \text{ erg s}^{-1}$ (Venturi et al., in prep.).

We note that the GA-NIFS survey also comprises additional AGN not included in this study: two of them have been originally selected for their dense environments, LBQS 0302–0019 (with its own secondary obscured AGN; see [13]) and BR1202–0725 (Carniani et al., in prep.); we therefore decided to exclude them from this work, as their inclusion would bias our sample. Six additional quasars at $z > 6$ (e.g. [28, 54]) have not been taken into account in this work because in these high- z sources the $[\text{N II}] \lambda 6583$ is very faint and usually undetected (likely due to their lower metallicity, e.g. [12, 37, 55]), hence precluding the use of BPT diagnostics to discover AGN emission in their companion sources; other diagnostics might be required (e.g. the detection of very faint $\text{He II } \lambda 4686$ and BLR lines in the optical spectra [10, 12, 56]) and we therefore defer this analysis to a forthcoming paper.

JWST/NIRSpec observations, and data reduction

The information about the NIRSpec observations is reported in Table A1. For all but two targets, we used the grating/filter pair G235H/F170LP. The sources HZ10 and GS3073 were observed with G395H/F290LP; GS539 was observed with both configurations. This setting was chosen in order to cover all main optical lines from $H\beta$ to $[\text{S II}] \lambda\lambda 6716, 31$ doublet lines with high spectral resolution ($R \sim 2700$).

Raw data files were downloaded from the MAST archive and subsequently processed with the JWST Science Calibration pipeline version 1.8.2 under CRDS context `jwst_1068.pmap`. We made several modifications to the default three-stages reduction to increase data quality, which are described in detail by [13] and briefly reported here. The individual count-rate frames were further processed at the end of the pipeline Stage1, to correct for different zero-level in the individual (dither) frames, and subtract the vertical $1/f$ noise. We masked regions that are affected by leakage from failed open shutters, and by persistence due to cosmic rays. The final cubes were combined using the *drizzle* method with pixel scales of $0.03''$, for which we used an official patch to correct a known bug. The small pixel scale is required to better identify close dual AGN, fully exploiting the spatial resolution of the data ([47]). We also patched the pipeline to avoid over-subtraction of elongated cosmic ray artefacts during the Stage1, and used a modified version of LACOSMIC ([57]) to reject strong outliers before the construction of the final data cube ([47]). The astrometric alignment of the NIRSpec data was computed relative to HST images that have been registered to Gaia DR3.

MUSE observations

Two out of the 17 systems in the GA-NIFS AGN sub-sample have archival VLT/-MUSE data, from the MUSE-WIDE ([58]) and the MUSE-UDF ([59]) surveys. These observations cover the rest-frame UV spectra of GS551 and GS10578, respectively. Reduced MUSE datacubes were downloaded from the MUSE-WIDE cut-out service¹, for the source GS551, and from the ESO archive, for GS10578. Their observational log is reported in Table A1. Because the MUSE spectrograph does not operate in vacuum and the wavelength calibration is in standard air, we converted them in vacuum before the fit analysis, consistent with NIRSpec. As for the case of NIRSpec observations, the astrometric alignment of the MUSE data was computed relative to HST images registered to Gaia DR3.

Analysis of NIRSpec data

JWST/NIRSpec observations revealed that most of our 17 AGN reside in complex environments, with evidence of gravitational interactions, and a number of $[\text{O III}]$ emitters within a few hundred km s^{-1} from the primary AGN. To investigate the nature of these $[\text{O III}]$ emitters, we extracted integrated spectra from 5×5 spaxel apertures centred at the peak position of all identified emitters (comprising the primary AGN),

¹<https://musewide.aip.de/cutout/>

hence from a region of $0.15'' \times 0.15''$ broadly corresponding to the spatial resolution element of NIRSPEC IFS observations ([47]).

We modelled their integrated spectra with a combination of Gaussian profiles. We fitted the most prominent gas emission lines by using the Levenberg-Marquardt least-squares fitting code CAP-MPFIT ([60]). In particular, we modelled the $H\alpha$ and $H\beta$ lines, the [O III] $\lambda\lambda 4959, 5007$, [N II] $\lambda\lambda 6548, 83$, and [S II] $\lambda\lambda 6716, 31$ doublets applying a simultaneous fitting procedure ([13]), so that all line features corresponding to a given kinematic component have the same velocity centroid and full width at half maximum (FWHM). The modelling of the $H\alpha$ and $H\beta$ BLR emission in GS1638-A required the use of broken power-law components (e.g. [61]): they are preferred to a combination of extremely broad Gaussian profiles, because the former tend to minimise the degeneracy between NLR and BLR emission. Finally, we use the theoretical model templates of [62] to reproduce the [Fe II] emission in the wavelength region $4000 - 5500 \text{ \AA}$. The final number of kinematic components used to model the spectra is derived on the basis of the Bayesian information criterion (BIC, [63]).

The continuum emission, when detected, is modelled with a low-order polynomial function, and subtracted prior to fitting the emission lines. For GS10578-A, which shows strong stellar continuum and absorption line features, we used the model obtained by [47].

The best-fit models are then used to infer the optical NLR line fluxes required for the BPT diagnostics (Fig. 2a), and identify the multiple AGN systems reported in this work. The presence of BLR emission and ionised outflows in individual sources is discussed in the following sections. Emission line ratios, [O III] and $H\alpha$ luminosities, and [O III] line widths are reported in Table A2.

Analysis of MUSE data

MUSE spectroscopic data are analysed following the same general procedures described in the previous section. In particular, we extracted the spectra of GS10578-A and LAE2 (Fig. 3) from the MUSE-UDF datacube. We used an aperture of 3×3 spaxels ($0.6'' \times 0.6''$) for GS10578-A, broadly corresponding to the spatial resolution of these data; a larger aperture of 5×5 spaxels was instead preferred for the LAE2 spectrum, to increase the S/N in the vicinity of the He II line. The fit analysis required the use of a single Gaussian profile for the lines He II $\lambda 1640$, C IV $\lambda\lambda 1549, 1550$, and C III] $\lambda\lambda 1907, 1909$ (with the latter two modelled taking into account their doublet nature), which are the lines required for the classification of AGN and SF galaxies according to the UV diagnostics proposed by [10, 11]. For the second target for which we employed MUSE observations, GS551, we similarly extracted a 3×3 spaxels integrated spectrum for GS551-A, and two additional spectra at the position of nearby Ly α emitters (see Fig. B3). We fitted the AGN emission lines with single Gaussian profiles, and applied the same UV diagnostics mentioned above; the two additional spectra do not show any other emission lines apart from Ly α . Also for these targets, the outcomes of the spectroscopic analysis are discussed in the following sections. Emission line ratios, He II luminosities, and line widths are reported in Table A2.

AGN bolometric luminosity

For all AGN detected with NIRSpect, we computed the bolometric luminosities from the narrow $H\beta$ line, under the assumption that this emission comes from the NLR; bolometric corrections were computed using Eq. 3 of [45] (assuming a mean accretion disk inclination of 56°). These luminosities were preferred to the [O III]-based ones, because the latter are more dependent on the SMBH properties and the ionisation parameter (e.g. [45]); [O III] (and $H\alpha$) luminosities are reported in Table A2 for each target presented in this work. All $H\beta$ luminosities have been corrected for extinction, using the measured Balmer decrements reported in Table A2 and assuming a [64] extinction law. For the AGN in LAE2 detected with MUSE we computed the bolometric luminosity from an upper limit on the (undetected) continuum emission at 1400\AA , using Eq. 3 by [45], considering a mean (56°) accretion disk inclination. We note that its He II luminosity is comparable with that of GS10578-A; this might suggest that LAE2 and the primary AGN have comparable bolometric luminosities. All bolometric luminosities are reported in Table 1.

Stellar masses of AGN Host Galaxies

To study the physical properties of the stellar populations in Enfield and Mr. West, we analysed the prism ($0.6\text{--}5.3\mu\text{m}$) NIRSpect IFS observations in a spaxel-by-spaxel basis following the method described in [65], and adapted to the modelling of NIRSpect IFS data by [47]. These data were reduced following the same procedure described above. Based on this method, we derived integrated stellar masses of $\sim 10^9 M_\odot$ for both AGN host galaxies, by adding all the spaxels associated with these systems. In particular, for Mr. West we considered a circular region with $r = 0.2''$ centred at the position of the nucleus (AGN-B in Fig. 1c), while for Enfield we considered a larger ($r = 0.3''$) region to encompass its ring-shaped structure (reddish region in Fig. 1c). More detailed analysis of the physical properties of the stellar populations in this very complex system will be presented in Pérez-González et al., in prep.; here we stress that the mass measurements depend only slightly on the chosen apertures.

For all other systems observed with NIRSpect IFS, we analysed through spectral energy distribution (SED) fitting the COSMOS (GOODS-S) UV-to-NIR multiwavelength photometry collected by [66] ([67]), and the far-IR data by [68] ([69]). We also included in the analysis the ALMA sub-millimeter detections (for COS1638) and 3σ upper limits (for all other sources). For the $\text{Ly}\alpha$ emitter in the vicinity of GS10578, associated with the AGN-C (Fig. 3), we used publicly available NIRCcam and HST measurements collected by ([70]). We modelled the SED with the Code Investigating GALaxy Emission (CIGALE [71], version 0.11.0), a publicly available state-of-the-art galaxy SED-fitting software. This code disentangles the AGN contribution from the emission of the host by adopting a multicomponent fitting approach and includes attenuated stellar emission, dust emission heated by star formation, AGN emission (both primary accretion disk emission and dust-heated emission), and nebular emission (see [72, 73] for further details). The more detailed SED analysis will be presented in Circosta et al., in prep. Here we report that the primary AGN are hosted in massive

($\approx 10^{11} M_{\odot}$) galaxies; the secondary and tertiary AGN hosts have smaller masses, in the range $10^8 - 10^{10} M_{\odot}$ (see Table 1). Unfortunately, no M_* measurements can be obtained for COS1638-B, GS551-B and GS10578-B, as they are not resolved as individual sources in the above mentioned catalogues (they are too close to the primary AGN): indeed, the photometry used for the primary AGN host may be contaminated by these companions; as a result, the estimates we obtain may include the contribution of both components.

A separate handling is required for the type 1 COS1638-A. Stellar mass estimates in the range $10^8 - 10^{12} M_{\odot}$ are reported in the literature for the host galaxy of the primary AGN (e.g. [66, 68]); this divergence is likely due to the non-thermal AGN emission dominating the optical continuum (Circosta et al, in prep.), which is precluding an SED-based estimate of M_* . However, an order of magnitude estimate of the stellar mass can be obtained considering our $M_{BH} = (4 \pm 1) \times 10^8 M_{\odot}$ measurement (see Extended material) and assuming the local black hole mass-stellar mass relation ([74]), $M_* \sim 10^{11} M_{\odot}$. A further independent estimate can be obtained for both primary and secondary AGN hosts from the far-IR-based dust mass $M_{dust} \sim 10^{11} M_{\odot}$ reported in [75] and referring to the dual AGN system (because of the poor spatial resolution of far-IR data): assuming that 62% of it is due to the AGN-B host (see Extended Data), and considering a conservative $M_{dust}/M_* = 0.02 \pm 0.01$ ([76]) we obtained $\log(M_*/M_{\odot}) \sim 10.9 \pm 0.4$, for COS1638-A, and $\sim 11.1 \pm 0.4$, for COS1638-B.

Intrinsic vs. external AGN ionization source

For two very close AGN pairs, GS551-A and -B with separation of 0.7 kpc, and GS10578-A and -B with separation of 4.7 kpc, we also checked whether the primary AGN can power the emission in the companion galaxy. Specifically, we tested whether the line emission in GS551-B and GS10578-B can be explained by an external ionisation source, or requires an intrinsic source (i.e. a secondary AGN).

Following [36], we derived a lower limit to the incident ionizing flux required for a line emitter taking into account the observed surface brightness in the recombination line $H\beta$, and its distance from the primary AGN. No corrections for projection effects are considered, to obtain conservative estimates: a given companion will always lie farther from the nucleus of the primary AGN than our projected measurement, and hence require a higher incident flux. In a simple approximation, we considered the companion to be circular in cross-section as seen from the nucleus, so its solid angle is derived as $\theta = 2 \arctan(r/d)$, where r is the radius of the emitting region and d is the angular distance from the primary nucleus. The required ionizing luminosity is given from the observed quantities as

$$L_{ion} > L(H\beta) \times k_{bol} \times \gamma \times \left(\frac{4\pi}{\theta^2} \right) \quad (1)$$

where $L(H\beta)$ is the $H\beta$ luminosity of the companion, k_{bol} is the bolometric correction from [45] (see above), $\gamma = 0.14$ is the fraction of bolometric to ionising luminosity (considering the mean radio-quiet SED, following [77]), and θ is the subtended angle (in steradian). This required ionising luminosity has to be compared with the incident ionizing luminosity coming from the primary AGN: $L_{inc} = L_{bol} \times \gamma$ (following [77]).

For GS551-B, we obtain a required $L_{ion} > 4 \times 10^{45}$ erg s⁻¹, slightly higher than the incident $L_{inc} = 10^{45}$ erg s⁻¹. Although L_{inc} and L_{ion} are of the same order of magnitude, and we cannot definitely exclude the possibility of an external AGN ionisation, the latter scenario is very unlikely. In fact, L_{ion} has to be considered as a lower limit: assuming a $3 \times$ larger physical distance, we would obtain $10 \times$ higher L_{ion} , definitely incompatible with external AGN ionization source. Therefore, our results are more likely compatible with an intrinsic ionisation, hence with the presence of a secondary AGN.

For GS10578-B, we obtain a required $L_{ion} > 3 \times 10^{45}$ erg s⁻¹, to be compared with the incident $L_{inc} \approx 6 \times 10^{43}$ erg s⁻¹. In this case, the ionising flux coming from the primary AGN is not enough to explain the emission in GS10578-B; we can therefore conclude that the latter is associated with a secondary AGN.

For the remaining sources, the required ionizing luminosity is $10\text{s} - 10^3 \times$ higher than the incident luminosity, definitely excluding the possibility of an external AGN ionization source. Similar computations are not required for the pair LAE2 – GS10578-A, as the two sources have comparable emission line luminosities in the UV (Table A3).

Shock ionization

We also ruled out the possibility that shocks could ionize the gas in the companions. Following [78], we used the shock model predictions of H α luminosity from MAPPING V ([79]), with magnetic field values in the range 1–10 μ G, shock velocities in the range 200–1000 km s⁻¹, pre-shock densities in the range 1–10 cm⁻³, and assuming a metallicity of 1 Z_{\odot} . These predicted luminosities are a factor of 4-to-2 dex smaller than our measurements (Table A2); therefore, we conclude that shock ionisation cannot be responsible for the emission in the secondary AGN.

Acknowledgments. We thank C. Vignali and E. Bronzini for useful discussion on the processing of *Chandra* data. We thank K. Nakajima for providing the theoretical model grids published by [10]. The project leading to this publication has received support from ORP, that is funded by the European Union’s Horizon 2020 research and innovation programme under grant agreement No 101004719 [ORP]. This work is based on observations taken by the MUSE-Wide Survey as part of the MUSE Consortium. This work has made use of data from the European Space Agency (ESA) mission *Gaia* (<https://www.cosmos.esa.int/gaia>), processed by the *Gaia* Data Processing and Analysis Consortium (DPAC, <https://www.cosmos.esa.int/web/gaia/dpac/consortium>). Funding for the DPAC has been provided by national institutions, in particular the institutions participating in the *Gaia* Multilateral Agreement.

MP, SA, and BRP acknowledge support from the research project PID2021-127718NB-I00 of the Spanish Ministry of Science and Innovation/State Agency of Research (MCIN/AEI/10.13039/501100011033). MP is further supported by the Programa Atracción de Talento de la Comunidad de Madrid via grant 2018-T2/TIC-11715. IL acknowledges support from PID2022-140483NB-C22 funded by AEI

10.13039/501100011033 and BDC 20221289 funded by MCIN by the Recovery, Transformation and Resilience Plan from the Spanish State, and by NextGenerationEU from the European Union through the Recovery and Resilience Facility. PGP-G acknowledges support grants PGC2018-093499-B-I00 and PID2022-139567NB-I00 funded by Spanish Ministerio de Ciencia e Innovación MCIN/AEI/10.13039/501100011033, FEDER, UE. FDE, TJL, RM and JS and acknowledge support by the Science and Technology Facilities Council (STFC), by the ERC Advanced Grant 695671 “QUENCH”, and by the UKRI Frontier Research grant RISEandFALL; RM is further supported by a research professorship from the Royal Society. AJB has received funding from the European Research Council (ERC) under the European Union’s Horizon 2020 Advanced Grant 789056 “First Galaxies” GC, MP, GV and EB acknowledge the support of the INAF Large Grant 2022 ”The metal circle: a new sharp view of the baryon cycle up to Cosmic Dawn with the latest generation IFU facilities”.

Author Contributions

MP led the NIRSpec data reduction and analysis, as well as the MUSE data processing, with input from several coauthors. MP wrote the paper, and developed the main interpretation of the results. IL processed the ALMA data of all multiple AGN systems, and performed the astrometric registration. CC performed the SED data analysis. EB processed the *Chandra* data. PPG inferred the stellar masses of Enfield and Mr. West galaxies. All authors discussed the results and commented on the manuscript.

Competing interests

The authors declare no competing interests.

Data availability

The data that support the findings of this study are available from the corresponding author upon request.

Code availability

We used the [Python](#) programming language, maintained and distributed by the Python Software Foundation. We further acknowledge direct use of [astropy](#), [matplotlib](#), [numpy](#), and [scipy](#).

Corresponding Author

Michele Perna (mperna@cab.inta-csic.es)

Extended Data A

We report the information about NIRSpec observations in Table [A1](#); Tables [A2](#) and [A3](#) outline the NIRSpec and MUSE fit results, respectively.

Figure A1 shows the integrated spectra of all [O III] emitters identified in Fig. 1, together with the best-fit spectra used to measure the flux ratios reported in the BPT diagram (Fig. 2a).

Table A1: Log of observations

target	RA DEC	instrument	program ID	Obs. date	Exposure (s)
COS349	150.0043771 2.03890	NIRSpec	1217	09-05-2023	3560
COS590	149.7554125 2.73853	NIRSpec	1217	09-05-2023	3560
COS1118	149.8791917 2.22584	NIRSpec	1217	23-04-2023	3560
COS1638*	150.7355417 2.19956	NIRSpec	1217	26-04-2023	3560
COS1656*	150.2715833 1.61385	NIRSpec	1217	21-04-2023	3560
COS2949	150.4029167 1.87889	NIRSpec	1217	23-04-2023	3560
HZ10	150.2471250 1.55534	NIRSpec	1217	22-05-2023	18207
Mr. West & Enfield*	150.0614600 2.37868	NIRSpec	1217	01-05-2023	15872
GS133	53.0206229 -27.74223	NIRSpec	1216	12-09-2022	3560
GS539	53.1220783 -27.93878	NIRSpec	1216	12-09-2022	3501
GS551*	53.1243458 -27.85163	NIRSpec	1216	12-09-2022	3560
		MUSE	094.A-0205	25-12-2014	3600
GS774	53.1744017 -27.86740	NIRSpec	1216	12-09-2022	3560
GS811	53.1846596 -27.88097	NIRSpec	1216	12-09-2022	3560
GS3073	53.0788554 -27.88416	NIRSpec	1216	25-09-2022	18207
GS10578*	53.1653058 -27.81413	NIRSpec	1216	12-08-2022	14706
		MUSE	1101.A-0127	mosaic ¹	340500
GS19293	53.0539287 -27.74771	NIRSpec	1216	06-02-2023	14706
GS20936	53.1178958 -27.73438	NIRSpec	1216	26-08-2022	14706

The multiple AGN systems presented in this work are marked with * symbols.

¹GS10578 MUSE-UDF observations obtained from a collection of different exposures, covering three semesters.

Extended Data B

Here we report a brief description of the main properties of each system studied in this work.

COS1638 (dual AGN)

COS1638 hosts a bright type 1 AGN with an X-ray luminosity $\log(L_{2-10 \text{ keV}}/\text{erg s}^{-1}) \sim 44.5$ ([52]). Its optical spectrum (Fig. A1a) shows prominent BLR emission in both $H\alpha$ and $H\beta$ lines, and strong iron emission in the vicinity of the [O III] lines. From the best-fit described in Methods, we derived $M_{BH} = (4 \pm 1) \times 10^8 M_{\odot}$, a BLR $H\beta$ -based bolometric luminosity $\log(L_{bol} / \text{erg s}^{-1}) = 46.5 \pm 0.1$ (using the Eqs. 38 and 25 by [80]), and hence an Eddington ratio of 0.8 ± 0.2 . These values have been obtained from the BLR $H\beta$ luminosity (corrected for extinction, $E(B-V) = 0.6$ from the BLR Balmer decrement, assuming a [64] extinction law), consistent with that inferred from the NLR and reported in Table 1.

Table A2: NIRSspec fit results

Target	σ (km s ⁻¹)	Log([O III]/H β)	Log([N II]/H α)	H α /H β	Log(L([O III])) (erg s ⁻¹)	Log(L(H α)) (erg s ⁻¹)
COS1638-A ¹	1200 ⁺⁴⁵ ₋₉₀	0.08 ^{+0.08} _{-0.03}	-0.45 ^{+0.51} _{-0.55}	6.4 ^{+2.1} _{-0.5}	42.6	42.9
COS1638-B	1030 ⁺¹²⁰ ₋₃₆	0.9 \pm 0.1	-0.1 ^{+0.5} _{-0.2}	9.1 ^{+8.0} _{-2.5}	41.8	42.0
GS551-A	406 ⁺²⁷ ₋₁₉	1.06 ^{+0.04} _{-0.02}	-0.35 ^{+0.19} _{-0.04}	3.67 ^{+0.54} _{-0.31}	43.1	42.6
GS551-B	195 ⁺²⁰ ₋₉	0.90 ^{+0.09} _{0.03}	-0.29 ^{+0.16} _{-0.18}	2.35 ^{+0.56} _{-0.39}	42.0	41.4
Enfield	130 \pm 3	0.91 ^{+0.08} _{-0.03}	-0.33 ^{+0.08} _{-0.05}	2.8 ^{+0.6} _{-0.3}	41.1	41.7
Mr. West	172 \pm 8	> 0.79	0.05 ^{+0.15} _{-0.07}	> 1	41.6	41.2
COS1656-A	666 ⁺¹⁰ ₋₆	0.99 ^{+0.07} _{-0.10}	-0.17 ^{+0.10} _{-0.11}	4.29 ^{+0.86} _{-1.15}	42.7	42.2
COS1656-B	144 \pm 7	0.61 ^{+0.08} _{-0.06}	-0.32 ^{+0.10} _{-0.08}	2.79 ^{+0.80} _{-0.35}	41.5	41.3
GS10578-A	730 \pm 10	1.01 ^{+0.07} _{-0.03}	0.61 ^{+0.08} _{-0.04}	3.23 ^{+0.70} _{-0.45}	42.1	41.6
GS10578-B	130 \pm 5	0.97 ^{+0.13} _{0.05}	-0.75 ^{+0.06} _{-0.1}	3.50 ^{+1.43} _{-0.25}	41.5	41.0

Best-fit spectroscopic results for the most prominent emission lines detected with NIRSspec. The velocity dispersion σ refers to the total [O III] emission line profile. [O III] and H α luminosities have typical uncertainty of 0.1 dex, and are not corrected for extinction.

¹COS1638-A flux ratios are not reported in Fig. 2a, as they are affected by degeneracy between NLR (systemic and outflow) and BLR emission; the presence of an AGN in this system is confirmed by the presence of BLR and extremely fast outflows (Fig. A1a).

Table A3: MUSE fit results

target	dv (km s ⁻¹)	σ (km s ⁻¹)	$\frac{CIII]}{HeII}$	$\frac{CIV}{HeII}$	$\frac{CIV}{CIII]}$	$\frac{CIII]+CIV}{HeII}$	L(He II) (erg s ⁻¹)
GS10578	-245 ⁺³⁶ ₋₂₄	405 ⁺¹³ ₋₈	0.15 ^{+0.04} _{-0.03}	0.31 ^{+0.04} _{-0.02}	0.16 ^{+0.04} _{-0.02}	0.54 ^{+0.04} _{-0.02}	40.8 \pm 0.1
LAE2	181 ⁺¹¹ ₋₁₀	140 \pm 7	-0.19 \pm 0.05	0.02 ^{+0.05} _{-0.03}	0.21 ^{+0.08} _{-0.01}	0.23 ^{+0.04} _{-0.02}	40.9 \pm 0.2
GS551	-2 ⁺¹⁰ ₋₃₀	590 \pm 40	0.15 \pm 0.05	0.58 ^{+0.04} _{-0.07}	0.39 ^{+0.14} _{-0.02}	0.71 ^{+0.04} _{-0.02}	41.4 \pm 0.1

Best-fit spectroscopic results for the most prominent emission lines detected with MUSE. dv is the velocity offset with respect to the optical (NIRSspec) zero-velocities in the primary AGN. Luminosities and flux ratios are in log-scale.

The secondary AGN (COS1638-B) shows very high [N II]/H α and [O III]/H β line ratios (Table A2), and extremely broad profiles with σ ([O III]) \sim 1100 km s⁻¹ (Fig. A1a). Such broad profiles cannot be due to starburst driven outflows (e.g. [81]); instead they are explained by the presence of energetic AGN outflows (e.g. [82]). [O III] emission is also detected between the primary and secondary AGN, indicating gravitational interactions (Fig. 1a). The complex morphology of this system, with different clumps at several kpc from the primary AGN host, is also observed with HST/ACS images (e.g. tracing rest-frame UV continuum). By analysing archival ALMA data (2016.1.00463.S, PI: Y. Matsuda) we found that COS1638-B is brighter than the primary AGN host at \sim 1 mm (obs-frame): we measured a total integrated flux of 11.4 mJy, with 62% of which associated with COS1638-B. Therefore, a significant amount of dust is located at the position of the secondary AGN, in line with the extreme Balmer decrement we measure in NIRSspec data (H α /H β \sim 9). Taking into account their relative ALMA

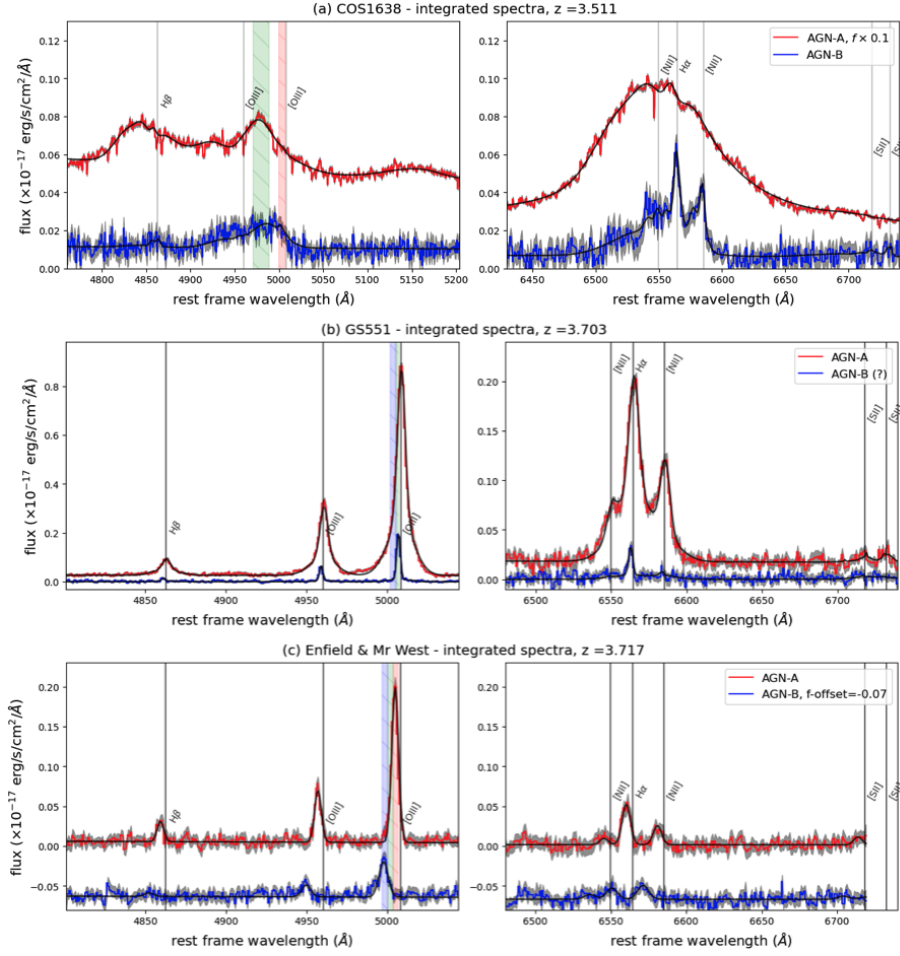


Fig. A1: (a) COS1638-A and B integrated spectra: spectra of the primary (red curve) and secondary (blue) AGN; the vertical green and red shaded areas correspond to the velocity channels used to generate the [O III] map and contours in Fig. 1a, respectively. Both targets present broad line profiles, due to powerful outflows. For visual purposes, the spectrum of the AGN-A has been re-scaled, as labeled. **(b) GS551-A and B Integrated spectra:** spectra of the two AGN, reporting the velocity channels used to generate Fig. 1b. The primary source GS551-A shows a strong outflow. **(c) Integrated spectra of Jekyll's companions:** spectra extracted from the boxes defined in Fig. 1c. The [O III] profiles of the two AGN show modest blue wings, possibly due to outflows; the H β line in AGN-B is detected at 2–3 σ . The vertical blue, green and red shaded regions correspond to the velocity channels used to generate the maps in Fig. 1c. For each spectrum, we report the best-fit profiles in black. The grey vertical lines indicate the rest-frame wavelength of the main optical lines at the systemic redshift of the primary AGN; for Jekyll's companions, we refer to the Jekyll systemic.

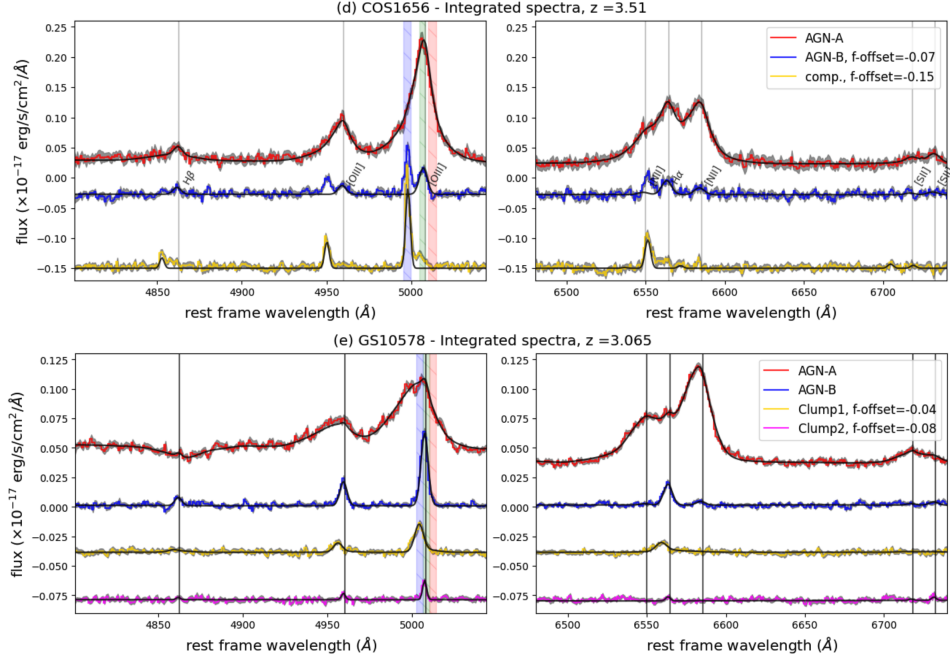


Fig. A1: continued. **(d) COS1656-A and B integrated spectra:** spectra of the two AGN (blue and red curves), and a bright extended structure (gold curve) close to AGN-B. For each spectrum, we also report the best-fit profiles in black. The primary AGN shows a strong outflow. The spectra of AGN-B and its close companion present double-peaked emission line profiles, as they partially overlap along our line of sight (see Fig. 1d). The best-fit profiles - and the inferred flux ratios reported in the BPT in Fig. 2a - present only the contributions due to the AGN-B in the blue spectrum, and due to the companion in the gold spectrum. **(e) Integrated spectra of GS10578-A and its close companions:** the spectra of the AGN-A and B are shown in red and blue; those of close clumps are represented in gold and purple, as labeled. For each spectrum, we report the best-fit profiles in black; for AGN-A, a pPXF best-fit model (from [47]) is used to reproduce the stellar continuum and absorption features. The vertical blue, green, and red shaded areas correspond to the velocity channels used to generate the [O III] map and contours in Fig. 1 (d and e panels). The grey vertical lines indicate the rest-frame wavelength of the main optical lines at the systemic redshift of the primary AGN.

continuum fluxes, and the CIGALE best-fit results, we also inferred the star-formation rate (SFR) of $\approx 1200 M_{\odot} \text{ yr}^{-1}$ for AGN-B, and $\approx 800 M_{\odot} \text{ yr}^{-1}$ for AGN-A.

We also inspected the X-ray morphology of this dual AGN through the *Chandra* exposures of the COSMOS-*Legacy* survey. Given the survey strategy [83, 84], the target is observed at different distances from the *Chandra* aim point in each exposure, with an off-axis angle of at least $\theta \sim 3.5'$. As a result, the single-exposure point

spread function (PSF) at the position of the primary AGN is of at least $\sim 1.2''$. We thus investigated the X-ray radial profile of COS1638 in the *Chandra* exposure in which it is observed in the best conditions (obsID 15253, $\theta \sim 3.5'$, PSF $\sim 1.2''$), using the Chandra Ray Tracer (ChaRT v.2²) online tool (see Fig. B2 for details). We simulated the *Chandra* PSF at the target position with ChaRT, feeding the ray-tracing code with the target and aim point coordinates, the exposure time and the best fit of the 0.3–7 keV source spectrum extracted from this observation. We ran 50 simulations using this setup, each of which was then projected on the detector plane using MARX v.5.5.2 [85]. We merged the output of all the simulations with the task `dmmerge` in CIAO v4.15 [86] to best reproduce the *Chandra* PSF. We then extracted the radial profile of COS1638 by using a set of 4 annuli ($\delta r \simeq 0.8\text{pix} \simeq 0.4''$) centered on the peak of the source emission (which corresponds to COS1638-A) and fitted it with the radial PSF model (obtained in a similar way) plus a constant set to the measured background level (model: PSF+constant), using Sherpa 4.15.1 [87]. Background contribution was estimated from a $15''$ -radius source-free circle in the proximity of our target. Figure B2 shows the 0.3–7 keV (observed-frame) *Chandra* image (right) together with a comparison between the observed X-ray radial profile and the simulated PSF. The observed profile shows hints ($\sim 2\sigma$) of an X-ray excess at the distance of COS1638-B (~ 2 -3 native Chandra pixels, corresponding to $\sim 1.2''$). Hence, despite the degraded PSF due to the off-axis position, the X-ray morphology suggests the presence of a second peak at the position of COS1638-B (see Fig. B2). We tested the possibility of this peak being due to high SF activity, rather than to a secondary AGN: the measured SFR $\simeq 1200 M_{\odot} \text{ yr}^{-1}$ (see Methods) translates to $L[0.5\text{-}8 \text{ keV}] \simeq 8 \times 10^{42} \text{ erg/s}$ ([88]). We thus addressed the detectability of a starburst galaxy with such high SFR, by assuming a reasonable spectral shape for the X-ray binary emission [89, and references therein]. The expected X-ray flux of such starburst galaxy would be almost one order of magnitude lower than the flux limit of COSMOS-*Legacy*, and further undetectable in obsID 15253 alone. Thus, the X-ray emission of COS1638 supports the presence of a secondary AGN in COS1638-B.

GS551 (dual AGN candidate)

GS551 is a massive ($\sim 10^{11} M_{\odot}$) galaxy hosting an obscured AGN. The NIRSpect IFS observations of GS551 are shown in Fig. 1b: we identified two bright [O III] emitters, one at the nuclear position of the central galaxy, dubbed GS551-A, and one at $\sim 0.4''$ north-west, dubbed GS551-B (also detected in HST-ACS and WFC3 images). In addition, diffuse [O III] emission at $\sim 5 \text{ kpc}$ on the east side of GS551 is detected.

The GS551-A spectrum (Fig. A1b) shows a strong outflow, and AGN emission line ratios, according to the standard BPT diagram (Fig. 2a). The second source similarly shows AGN line ratios, with ~ 10 times fainter features likely powered by intrinsic ionization of an obscured AGN (see Methods).

The 7MS *Chandra* observations do not allow the identification of the dual AGN, as their spatial separation is lower than the *Chandra* resolution at the position of the target; the (absorption-corrected, $N_{\text{H}} = 9 \pm 1 \times 10^{23} \text{ cm}^{-2}$) X-ray luminosity

²<https://cxc.cfa.harvard.edu/ciao/PSFs/chart2/runchart.html>

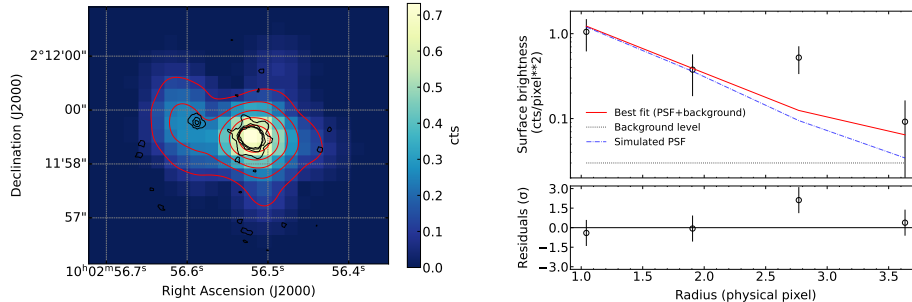


Fig. B2: COS1638 X-ray emission: Smoothed and sub-binned ($1/2$ pixel binning, i.e. $0.25''$ pixel scale) $0.3\text{--}7$ keV (observed-frame) image from the *Chandra* observation obsID 15253. NIRSpec [O III] contours are overlaid in black and X-ray contours in red. **COS1638 X-ray radial profile:** radial profile of COS1638 in obsID 15253 obtained from a set of 4 annuli ($\delta r \simeq 0.8\text{pix} \simeq 0.4''$) centered on the peak of the source emission (which corresponds to COS1638-A), and fitted it with the radial PSF model (see Extended data B) plus a constant set to the measured background level (model: PSF+constant), using Sherpa 4.15.1 [87]. The red solid line shows the best fit, the blue dash-dotted line shows the simulated PSF profile, while the black dotted line shows the measured background level. The observed radial profile shows hints ($\sim 2\sigma$) of an X-ray excess at the distance of COS1638-B ($\sim 2\text{--}3$ native Chandra pixels, corresponding to $\sim 1.2''$). Thus, despite the low count statistics and the degraded PSF due to the off-axis position, the X-ray morphology suggests the presence of a second peak at the position of COS1638-B.

$\log(L_{0.5\text{--}7\text{ keV}}/\text{erg s}^{-1}) = 44.35 \pm 0.05$ reported by [90] may therefore be attributed to both sources.

The characterisation of the GS551 Ly α nebula has been presented in [91, 92]. Here we highlight that GS551 shows a very complex Ly α halo on scales of ~ 15 kpc; interestingly, we also detected two additional Ly α structures ~ 20 kpc south-east and ~ 40 kpc north-west of the central galaxy, and at similar redshifts, as shown in Fig. B3. This indicates that GS551 resides in a complex environment, compatible with the presence of a secondary AGN in GS551-B.

Jekyll & Hyde companions: Enfield and Mr. West (dual AGN)

The galaxy ZF-20115 ([51]) is a post-starburst galaxy at $z \sim 3.7$ that exhibits a strong Balmer break and absorption lines. The far-infrared imaging reveals a luminous starburst located $\sim 0.4''$ (~ 3 kpc in projection) from the position of the rest-frame UV/optical emission, with an obscured star-formation rate of $100 M_{\odot} \text{ yr}^{-1}$ ([93]). The post-starburst and starburst galaxies were dubbed Jekyll and Hyde, respectively, by [51].

NIRSpec IFS observations reveal the presence of additional companions in the surroundings of Jekyll and Hyde: streams and clumpy structures are observed in both rest-frame optical continuum and emission lines (Fig. 1c). We identified two regions,

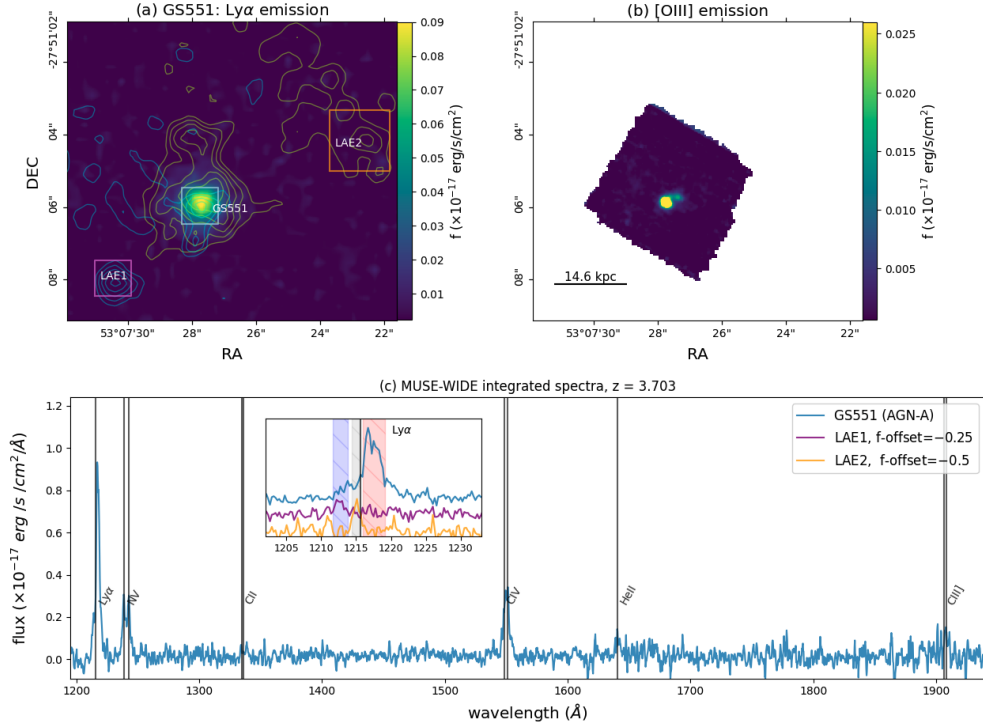


Fig. B3: (a) Ly α emitters in the vicinity of the GS551 dual AGN candidate. Ly α map obtained from MUSE cube, tracing emitting gas with $v \in [50, 900]$ km s $^{-1}$ from the GS551 systemic; the yellow (blue) contours indicate the Ly α emission at $v \in [-350, 50]$ km s $^{-1}$ ($v \in [-1050, -400]$ km s $^{-1}$) and highlight the presence of two nearby sources, labeled as LAE1 and LAE2. **(b) [O III] emitters:** the NIRSspec [O III] map, obtained integrating over the velocity range $v \in [-350, +350]$ km s $^{-1}$ from the GS551 systemic, shows two point-like sources already identified in Fig. 1b. **(c) MUSE spectra:** The GS551 spectrum has been smoothed for plotting purposes with a binning factor of 4; it shows strong AGN emission lines, such as C IV and He II, according to the [11] and [10] flux ratio diagnostics. The inset compares the Ly α profiles of GS551, LAE1 and LAE2; it also shows the vertical red shaded area used to generate the map in panel a, and the blue and grey shaded regions used for the contours. The three spectra have been extracted from the boxes indicated in the panel a, and reported to the rest-frame of GS551.

on the north-east and west sides of Hyde, associated with AGN line ratios (Fig. 2a). These two sources are dubbed Enfield (hosting AGN-A) and Mr. West (hosting AGN-B), following Pérez-González et al., in prep.. A detailed investigation of the stellar population properties within this dense system will be presented in Pérez-González et al., in prep.; here we report the stellar mass measurements for the two AGN host galaxies, of $\log(M_*) = 9.5 \pm 0.2$ (Enfield), and $= 9.4 \pm 0.3$ (see Methods).

In support of the presence of a dual AGN, we also report the presence of broad blue wings in the emission lines at the position of the two AGN (up to $\sim 300 - 400 \text{ km s}^{-1}$, see Fig. A1c), possibly associated with outflows or, alternatively, to tidal interactions between the active galaxies and Jekyll & Hyde.

No X-ray emission is detected in the surroundings of this complex system; we therefore measured the upper limit on the 0.3–7 keV flux from the *Chandra* COSMOS-Legacy mosaic ([52]) as follows. We derive the net count rate by using as source region the circularized median of the *Chandra* PSFs at the position of Jekyll from each exposure ($\sim 4.2''$) and a source-free circle of $15''$ -radius in the proximity of the target as background region. By assuming a photon index $\Gamma = 1.8$, we obtain $f_{0.3-7 \text{ keV}} = 1 \times 10^{-16} \text{ erg s}^{-1} \text{ cm}^{-2}$. Because of the size of the *Chandra* PSF ($\sim 4.2''$) at the position of Jekyll, this upper limit refers to both AGN we identified with NIRSPEC.

GS10578 & LAE2 (triple AGN)

GS10578 is a massive ($\sim 10^{11} M_{\odot}$), post-starburst galaxy at $z \sim 3.06$, merging with lower-mass, gas-laden satellites ([47]); it also hosts an obscured AGN with a column density $N_{\text{H}} = (5 \pm 4) \times 10^{23} \text{ cm}^{-2}$ and an X-ray luminosity $\log(L_{2-10\text{keV}}/\text{erg s}^{-1}) = 44.62 \pm 0.06$ ([90]). The inspection of archival MUSE observations allowed us to detect for the first time the extended Ly α halo surrounding GS10578, as well as two additional Ly α emitters (LAE1 and LAE2) connected with GS10578 (i.e. at same redshift, see Fig. 3); these structures are $\sim 50 \text{ kpc}$ (and $\sim 6000 \text{ km s}^{-1}$) from another Ly α halo discovered by [44].

The characterization of the Ly α halo surrounding GS10578 goes beyond the scope of this work. Here we focus on the study of the bright UV emission lines visible in the spectrum of GS10578, showing a double-peaked Ly α line, as well as the [N V], C IV, He II and C III] transitions, and the spectrum of the LAE2, with similar emission line features. The system LAE1, instead, is fainter and its spectrum only presents a Ly α line at the same redshift of GS10578 and LAE2 (within a few 100 km s^{-1}). The spectra of GS10578 and LAE2 are reported in Fig. 3. From the modelling of the emission lines in LAE2 and GS10578, we inferred the flux ratios reported in Table A3; these measurements are consistent with AGN ionisation, according to the UV diagnostics by [10] (Fig. 2b) and [11]. We note that the C III] might be affected by atmospheric sky line residuals (see the 1σ error curve associated with the LAE2 spectrum in the inset in Fig. 3c); however, the AGN classification is guaranteed even considering a 3σ upper limit for C III] (i.e. assuming that this line is undetected), or using the [11] diagnostics.

LAE1 and LAE2 have been also detected in JADES ([70]), and identified with the ID 253554 and ID 197907, but associated with photometric redshift $z_{ph} = 0.49$ and 0.33 , respectively. We used JADES photometry to determine the stellar mass of the Ly α emitter hosting the AGN-C, $\log(M_{*}) = 8.3 \pm 0.4$ (see Methods). LAE2 is not detected in 7 MS *Chandra* observations ([53]). Using the background map released by [53] we derived an X-ray upper limit for LAE2 (AGN-C) as done for the Lanyon & Enfield AGN pair (median PSF: $\sim 2''$; $\Gamma = 1.8$): $f_{0.3-7 \text{ keV}} = 9 \times 10^{-18} \text{ erg s}^{-1} \text{ cm}^{-2}$.

NIRSpec IFS observations cover a significant portion of the GS10578 Ly α halo, but not LAE1 and LAE2 (see Fig. 3). These observations allowed us to discover three [O III] emitters in the surrounding of the primary AGN: the brightest one hosts a secondary AGN (AGN-B in Fig. 1e), according to the BPT diagnostics. Being this source very close to the primary AGN (~ 4.7 kpc), we tested whether the GS10578-B emission can be due to intrinsic or external ionisation source. We favoured the former scenario, as the primary AGN is not powerful enough to ionise the gas at the position of GS10578-B (see Methods). Being this source very close to the primary AGN, it is likely that the X-ray luminosity inferred by [90] may be contaminated by the AGN-B emission.

All in all, the presence of a secondary and a tertiary AGN $\sim 0.7''$ and $\sim 3.6''$ of the GS10578 active nucleus, respectively, of the close LAE1 source, and a further relatively close (~ 50 kpc) extended LAE make this system an excellent laboratory to study the early phases of a cluster in formation at $z \sim 3$.

COS1656 (AGN pair)

COS1656 is a massive ($\sim 10^{11} M_{\odot}$) galaxy at $z \sim 3.5$. The NIRSpec IFS observations (Fig. 1d) reveal two additional bright [O III] emitters at ~ 10 kpc north from the primary AGN.

The spectra of the three targets are shown in Fig. A1d: COS1656-A presents a strong outflow ($\sigma([\text{O III}]) \sim 700 \text{ km s}^{-1}$), while the other two sources show double-peaked emission lines. This is due to the partial overlap of the two [O III] emitters along our line of sight. According to the BPT diagnostics, the northern system is associated with a secondary AGN, with bright [O III], H α and [N II] lines. This secondary AGN possibly contributes to the X-ray emission of COS1656 since the two sources are blended in the 7 MS CDFS data ([53]). The ionisation source of the close companion of AGN-B, instead, cannot be determined, because of the undetected [N II] (see orange circle in Fig. 2a).

The secondary AGN is fairly detected in HST/ACS images, and associated with a stellar mass $M_{\star} = 9.7 \pm 0.3$ (see also [66]). We note however that this measurement should be considered as an upper limit, because of the possible presence of two distinct systems on the LOS, see Fig. 1d.

The *Chandra* COSMOS Legacy observations do not allow the identification of the dual AGN, as their spatial separation is lower than the *Chandra* resolution at the position of the target ($6''$); the X-ray luminosity $\log(L_{2-10 \text{ keV}}/\text{erg s}^{-1}) = 44.4$ reported by [52] may therefore be attributed to both sources.

References

- [1] Blumenthal, G.R., Faber, S.M., Primack, J.R., Rees, M.J.: Formation of galaxies and large-scale structure with cold dark matter. *Nature* **311**, 517–525 (1984) <https://doi.org/10.1038/311517a0>

- [2] Capelo, P.R., Dotti, M., Volonteri, M., Mayer, L., Bellovary, J.M., Shen, S.: A survey of dual active galactic nuclei in simulations of galaxy mergers: frequency and properties. *MNRAS* **469**(4), 4437–4454 (2017) <https://doi.org/10.1093/mnras/stx1067> [arXiv:1611.09244](https://arxiv.org/abs/1611.09244) [astro-ph.GA]
- [3] De Rosa, A., Vignali, C., Bogdanović, T., Capelo, P.R., Charisi, M., Dotti, M., Husemann, B., Lusso, E., Mayer, L., Paragi, Z., Runnoe, J., Sesana, A., Steinborn, L., Bianchi, S., Colpi, M., del Valle, L., Frey, S., Gabányi, K.É., Giustini, M., Guainazzi, M., Haiman, Z., Herrera Ruiz, N., Herrero-Illana, R., Iwasawa, K., Komossa, S., Lena, D., Loiseau, N., Perez-Torres, M., Piconcelli, E., Volonteri, M.: The quest for dual and binary supermassive black holes: A multi-messenger view. *New Astron. Rev.* **86**, 101525 (2019) <https://doi.org/10.1016/j.newar.2020.101525> [arXiv:2001.06293](https://arxiv.org/abs/2001.06293) [astro-ph.GA]
- [4] Volonteri, M., Pfister, H., Beckmann, R., Dotti, M., Dubois, Y., Massonneau, W., Musoke, G., Tremmel, M.: Dual AGN in the Horizon-AGN simulation and their link to galaxy and massive black hole mergers, with an excursus on multiple AGN. *MNRAS* **514**(1), 640–656 (2022) <https://doi.org/10.1093/mnras/stac1217> [arXiv:2112.07193](https://arxiv.org/abs/2112.07193) [astro-ph.GA]
- [5] Chen, N., Di Matteo, T., Ni, Y., Tremmel, M., DeGraf, C., Shen, Y., Holgado, A.M., Bird, S., Croft, R., Feng, Y.: Properties and evolution of dual and offset AGN in the ASTRID simulation at z 2. *MNRAS* **522**(2), 1895–1913 (2023) <https://doi.org/10.1093/mnras/stad834> [arXiv:2208.04970](https://arxiv.org/abs/2208.04970) [astro-ph.GA]
- [6] Lemon, C., Anguita, T., Auger-Williams, M.W., Courbin, F., Galan, A., McMahon, R., Neira, F., Oguri, M., Schechter, P., Shajib, A., Treu, T., Agnello, A., Spiniello, C.: Gravitationally lensed quasars in Gaia - IV. 150 new lenses, quasar pairs, and projected quasars. *MNRAS* **520**(3), 3305–3328 (2023) <https://doi.org/10.1093/mnras/stac3721> [arXiv:2206.07714](https://arxiv.org/abs/2206.07714) [astro-ph.GA]
- [7] Mannucci, F., Pancino, E., Belfiore, F., Cicone, C., Ciurlo, A., Cresci, G., Lusso, E., Marasco, A., Marconi, A., Nardini, E., Pinna, E., Severgnini, P., Saracco, P., Tozzi, G., Yeh, S.: Unveiling the population of dual and lensed active galactic nuclei at sub-arcsec separations. *Nature Astronomy* **6**, 1185–1192 (2022) <https://doi.org/10.1038/s41550-022-01761-5> [arXiv:2203.11234](https://arxiv.org/abs/2203.11234) [astro-ph.GA]
- [8] Mannucci, F., Scialpi, M., Ciurlo, A., Yeh, S., Marconcini, C., Tozzi, G., Cresci, G., Marconi, A., Amiri, A., Belfiore, F., Carniani, S., Cicone, C., Nardini, E., Pancino, E., Rubinur, K., Severgnini, P., Ulivi, L., Venturi, G., Vignali, C., Volonteri, M., Pinna, E., Rossi, F., Puglisi, A., Agapito, G., Plantet, C., Ghose, E., Carbonaro, L., Xompero, M., Grani, P., Esposito, S., Power, J., Guerra Ramon, J.C., Lefebvre, M., Cavallaro, A., Davies, R., Riccardi, A., Macintosh, M., Taylor, W., Dolci, M., Baruffolo, A., Feuchtgruber, H., Kravchenko, K., Rau, C., Sturm, E., Wierorrek, E., Dallilar, Y., Kenworthy, M.: GMP-selected dual and lensed AGNs: selection function and classification based on near-IR

- colors and resolved spectra from VLT/ERIS, KECK/OSIRIS, and LBT/LUCI. arXiv e-prints, 2305–07396 (2023) <https://doi.org/10.48550/arXiv.2305.07396> [astro-ph.GA]
- [9] Baldwin, J.A., Phillips, M.M., Terlevich, R.: Classification parameters for the emission-line spectra of extragalactic objects. *PASP* **93**, 5–19 (1981)
- [10] Nakajima, K., Maiolino, R.: Diagnostics for PopIII galaxies and direct collapse black holes in the early universe. *MNRAS* **513**(4), 5134–5147 (2022) <https://doi.org/10.1093/mnras/stac1242> arXiv:2204.11870 [astro-ph.GA]
- [11] Feltre, A., Charlot, S., Gutkin, J.: Nuclear activity versus star formation: emission-line diagnostics at ultraviolet and optical wavelengths. *MNRAS* **456**(3), 3354–3374 (2016) <https://doi.org/10.1093/mnras/stv2794> arXiv:1511.08217 [astro-ph.GA]
- [12] Übler, H., Maiolino, R., Curtis-Lake, E., Pérez-González, P.G., Curti, M., Arribas, S., Charlot, S., Perna, M., Marshall, M.A., D’Eugenio, F., Scholtz, J., Bunker, A., Carniani, S., Ferruit, P., Jakobsen, P., Rix, H.-W., Rodríguez Del Pino, B., Willott, C.J., Böker, T., Cresci, G., Jones, G.C., Kumari, N., Rawle, T.: A massive black hole in a low-metallicity AGN at $z \sim 5.55$ revealed by JWST/NIRSpec IFS. arXiv e-prints, 2302–06647 (2023) <https://doi.org/10.48550/arXiv.2302.06647> [astro-ph.GA]
- [13] Perna, M., Arribas, S., Marshall, M., D’Eugenio, F., Übler, H., Bunker, A., Charlot, S., Carniani, S., Jakobsen, P., Maiolino, R., Rodríguez Del Pino, B., Willott, C.J., Böker, T., Circosta, C., Cresci, G., Curti, M., Husemann, B., Kumari, N., Lamperti, I., Pérez-González, P.G., Scholtz, J.: The ultradense, interacting environment of a dual AGN at $z \sim 3.3$ revealed by JWST/NIRSpec IFS. arXiv e-prints, 2304–06756 (2023) <https://doi.org/10.48550/arXiv.2304.06756> [astro-ph.GA]
- [14] Magorrian, J., Tremaine, S., Richstone, D., Bender, R., Bower, G., Dressler, A., Faber, S.M., Gebhardt, K., Green, R., Grillmair, C., Kormendy, J., Lauer, T.: The Demography of Massive Dark Objects in Galaxy Centers. *AJ* **115**, 2285–2305 (1998) <https://doi.org/10.1086/300353> astro-ph/9708072
- [15] Koss, M., Mushotzky, R., Treister, E., Veilleux, S., Vasudevan, R., Trippe, M.: Understanding Dual Active Galactic Nucleus Activation in the nearby Universe. *ApJ* **746**(2), 22 (2012) <https://doi.org/10.1088/2041-8205/746/2/L22> arXiv:1201.2944 [astro-ph.HE]
- [16] Shields, G.A., Rosario, D.J., Junkkarinen, V., Chapman, S.C., Bonning, E.W., Chiba, T.: LBQS 0103-2753: A Binary Quasar in a Major Merger. *ApJ* **744**(2), 151 (2012) <https://doi.org/10.1088/0004-637X/744/2/151> arXiv:1109.1524 [astro-ph.CO]

- [17] Husemann, B., Worseck, G., Arrigoni-Battaia, F., Shanks, T.: Discovery of a dual AGN at $z = 3.3$ with 20 kpc separation. *A&A* **610**, 7 (2018) <https://doi.org/10.1051/0004-6361/201732457> [astro-ph.GA]
- [18] Gaia Collaboration, Brown, A.G.A., Vallenari, A., Prusti, T., de Bruijne, J.H.J., Babusiaux, C., Bailer-Jones, C.A.L., Biermann, M., Evans, D.W., Eyer, L., Jansen, F., Jordi, C., Klioner, S.A., Lammers, U., Lindegren, L., Luri, X., Mignard, F., Panem, C., Pourbaix, D., Randich, S., Sartoretti, P., Siddiqui, H.I., Soubiran, C., van Leeuwen, F., Walton, N.A., Arenou, F., Bastian, U., Cropper, M., Drimmel, R.e.a.: Gaia Data Release 2. Summary of the contents and survey properties. *A&A* **616**, 1 (2018) <https://doi.org/10.1051/0004-6361/201833051> [arXiv:1804.09365](https://arxiv.org/abs/1804.09365) [astro-ph.GA]
- [19] Hwang, H.-C., Shen, Y., Zakamska, N., Liu, X.: Varstrometry for Off-nucleus and Dual Subkiloparsec AGN (VODKA): Methodology and Initial Results with Gaia DR2. *ApJ* **888**(2), 73 (2020) <https://doi.org/10.3847/1538-4357/ab5c1a> [arXiv:1908.02292](https://arxiv.org/abs/1908.02292) [astro-ph.GA]
- [20] Hopkins, P.F., Torrey, P., Faucher-Giguère, C.-A., Quataert, E., Murray, N.: Stellar and quasar feedback in concert: effects on AGN accretion, obscuration, and outflows. *MNRAS* **458**(1), 816–831 (2016) <https://doi.org/10.1093/mnras/stw289> [arXiv:1504.05209](https://arxiv.org/abs/1504.05209) [astro-ph.GA]
- [21] Ricci, C., Bauer, F.E., Treister, E., Schawinski, K., Privon, G.C., Blecha, L., Arevalo, P., Armus, L., Harrison, F., Ho, L.C., Iwasawa, K., Sanders, D.B., Stern, D.: Growing supermassive black holes in the late stages of galaxy mergers are heavily obscured. *MNRAS* **468**(2), 1273–1299 (2017) <https://doi.org/10.1093/mnras/stx173> [arXiv:1701.04825](https://arxiv.org/abs/1701.04825) [astro-ph.HE]
- [22] Perna, M., Sargent, M.T., Brusa, M., Daddi, E., Feruglio, C., Cresci, G., Lanzuisi, G., Lusso, E., Comastri, A., Coogan, R.T., D’Amato, Q., Gilli, R., Piconcelli, E., Vignali, C.: Molecular gas content in obscured AGN at $z \lesssim 1$. *A&A* **619**, 90 (2018) <https://doi.org/10.1051/0004-6361/201833040> [arXiv:1807.03378](https://arxiv.org/abs/1807.03378) [astro-ph.GA]
- [23] Koss, M.J., Blecha, L., Bernhard, P., Hung, C.-L., Lu, J.R., Trakhtenbrot, B., Treister, E., Weigel, A., Sartori, L.F., Mushotzky, R., Schawinski, K., Ricci, C., Veilleux, S., Sanders, D.B.: A population of luminous accreting black holes with hidden mergers. *Nature* **563**(7730), 214–216 (2018) <https://doi.org/10.1038/s41586-018-0652-7> [arXiv:1811.03641](https://arxiv.org/abs/1811.03641) [astro-ph.GA]
- [24] Rigby, J., Perrin, M., McElwain, M., Kimble, R., Friedman, S., Lallo, M., Doyon, R., Feinberg, L., Ferruit, P., Glasse, A., Rieke, M., Rieke, G., Wright, G., Willott, C., Colon, K., Milam, S., Neff, S., Stark, C., Valenti, J., Abell, J., Abney, F., Abul-Huda, Y., Acton, D.S., Adams, E., Adler, D., Aguilar, J., Ahmed, N., Albert, L., Alberts, S., Aldridge, D., Allen, M., Altenburg, M., al.: The Science Performance of JWST as Characterized in Commissioning. *PASP* **135**(1046), 048001 (2023) <https://doi.org/10.1088/1538-3873/acb293> [arXiv:2207.05632](https://arxiv.org/abs/2207.05632) [astro-ph.IM]

- [25] Jakobsen, P., Ferruit, P., Oliveira, C.A., Arribas, S., Bagnasco, G., Barho, R., Beck, T.L., Birkmann, S., Böker, T., Bunker, A.J., Charlot, S., Jong, P., Marchi, G., Ehrenwinkler, R., Falcolini, M., Fels, R., Franx, M., Franz, D., Funke, M., Giardino, G., Gnata, X., Holota, W., Honnen, K., Jensen, P.L., Jentsch, M., Johnson, T., Jollet, D., Karl, H., Kling, G., Köhler, J., Kolm, M.-G., Kumari, N., Lander, M.E., Lemke, R., López-Caniego, M., Lützgendorf, N., Maiolino, R., Manjavacas, E., Marston, A., Maschmann, M., Maurer, R., Messerschmidt, B., Moseley, S.H., Mosner, P., Mott, D.B., Muzerolle, J., Pirzkal, N., Pittet, J.-F., Pitzke, A., Posselt, W., Rapp, B., Rauscher, B.J., Rawle, T., Rix, H.-W., Rödel, A., Rumler, P., Sabbi, E., Salvignol, J.-C., Schmid, T., Sirianni, M., Smith, C., Strada, P., Plate, M., Valenti, J., Wettemann, T., Wiehe, T., Wiesmayer, M., Willott, C.J., Wright, R., Zeidler, P., Zincke, C.: The near-infrared spectrograph (NIRSpec) on the *James Webb* space telescope. *A&A* **661**, 80 (2022) <https://doi.org/10.1051/0004-6361/202142663>
- [26] Böker, T., Arribas, S., Lützgendorf, N., Oliveira, C.A., Beck, T.L., Birkmann, S., Bunker, A.J., Charlot, S., Marchi, G., Ferruit, P., Giardino, G., Jakobsen, P., Kumari, N., López-Caniego, M., Maiolino, R., Manjavacas, E., Marston, A., Moseley, S.H., Muzerolle, J., Ogle, P., Pirzkal, N., Rauscher, B., Rawle, T., Rix, H.-W., Sabbi, E., Sargent, B., Sirianni, M., Plate, M., Valenti, J., Willott, C.J., Zeidler, P.: The near-infrared spectrograph (NIRSpec) on the *James Webb* space telescope. *A&A* **661**, 82 (2022) <https://doi.org/10.1051/0004-6361/202142589>
- [27] Greene, T.P., Kelly, D.M., Stansberry, J., Leisenring, J., Egami, E., Schlawin, E., Chu, L., Hodapp, K.W., Rieke, M.: $\lambda = 2.4$ to $5 \mu\text{m}$ spectroscopy with the James Webb Space Telescope NIRCам instrument. *Journal of Astronomical Telescopes, Instruments, and Systems* **3**, 035001 (2017) <https://doi.org/10.1117/1.JATIS.3.3.035001>
- [28] Marshall, M.A., Perna, M., Willott, C.J., Maiolino, R., Scholtz, J., Übler, H., Carniani, S., Arribas, S., Lützgendorf, N., Bunker, A.J., Charlot, S., Ferruit, P., Jakobsen, P., Rodríguez Del Pino, B., Böker, T., Cameron, A.J., Cresci, G., Curtis-Lake, E., Jones, G.C., Kumari, N., Pérez-González, P.G.: Black hole and host galaxy properties of two $z \simeq 6.8$ quasars from the NIRSpec IFU. *arXiv e-prints*, 2302–04795 (2023) <https://doi.org/10.48550/arXiv.2302.04795> [arXiv:2302.04795](https://arxiv.org/abs/2302.04795) [astro-ph.GA]
- [29] Kashino, D., Lilly, S.J., Matthee, J., Eilers, A.-C., Mackenzie, R., Bordoloi, R., Simcoe, R.A.: Eiger i. a large sample of [oiii]-emitting galaxies at $5.3 < z < 6.9$ and direct evidence for local reionization by galaxies (2022) [arXiv:2211.08254](https://arxiv.org/abs/2211.08254) [astro-ph.GA]
- [30] Yang, J., Wang, F., Fan, X., Hennawi, J.F., Barth, A.J., Bañados, E., Sun, F., Liu, W., Cai, Z., Jiang, L., Li, Z., Onoue, M., Schindler, J.-T., Shen, Y., Wu, Y., Bhowmick, A.K., Bieri, R., Blecha, L., Bosman, S., Champagne, J.B., Colina, L., Connor, T., Costa, T., Davies, F.B., Decarli, R., De Rosa, G., Drake, A.B.,

- Egami, E., Eilers, A.-C., Evans, A.E., Farina, E.P., Habouzit, M., Haiman, Z., Jin, X., Jun, H.D., Kakiichi, K., Khusanova, Y., Kulkarni, G., Loiacono, F., Lupi, A., Mazzucchelli, C., Pan, Z., Rojas-Ruiz, S., Strauss, M.A., Tee, W.L., Trakhtenbrot, B., Trebitsch, M., Venemans, B., Vestergaard, M., Volonteri, M., Walter, F., Xie, Z.-L., Yue, M., Zhang, H., Zhang, H., Zou, S.: A SPectroscopic Survey of Biased Halos in the Reionization Era (ASPIRE): A First Look at the Rest-frame Optical Spectra of $z \lesssim 6.5$ Quasars Using JWST. *ApJ* **951**(1), 5 (2023) <https://doi.org/10.3847/2041-8213/acc9c8> [arXiv:2304.09888](https://arxiv.org/abs/2304.09888) [astro-ph.GA]
- [31] Giavalisco, M., Ferguson, H.C., Koekemoer, A.M., Dickinson, M., Alexander, D.M., Bauer, F.E., Bergeron, J., Biagetti, C., Brandt, W.N., Casertano, S., Cesarsky, C., Chatzichristou, E., Conselice, C., Cristiani, S., Costa, L.D., Dahlen, T., Mello, D., Eisenhardt, P., Erben, T., Fall, S.M., Fassnacht, C., Fosbury, R., Fruchter, A., Gardner, J.P., Grogin, N., Hook, R.N., Hornschemeier, A.E., Idzi, R., Jogee, S., Kretchmer, C., Laidler, V., Lee, K.S., Livio, M., Lucas, R., Madau, P., Mobasher, B., Moustakas, L.A., Nonino, M., Padovani, P., Papovich, C., Park, Y., Ravindranath, S., Renzini, A., Richardson, M., Riess, A., Rosati, P., Schirmer, M., Schreier, E., Somerville, R.S., Spinrad, H., Stern, D., Stiavelli, M., Strolger, L., Urry, C.M., Vandame, B., Williams, R., Wolf, C.: The great observatories origins deep survey: Initial results from optical and near-infrared imaging. *ApJ* **600**(2), 93–98 (2004) <https://doi.org/10.1086/379232>
- [32] Scoville, N., Aussel, H., Brusa, M., Capak, P., Carollo, C.M., Elvis, M., Giavalisco, M., Guzzo, L., Hasinger, G., Impey, C., Kneib, J.-P., LeFevre, O., Lilly, S.J., Mobasher, B., Renzini, A., Rich, R.M., Sanders, D.B., Schinnerer, E., Schminovich, D., Shopbell, P., Taniguchi, Y., Tyson, N.D.: The Cosmic Evolution Survey (COSMOS): Overview. *ApJS* **172**, 1–8 (2007) <https://doi.org/10.1086/516585> [arXiv:astro-ph/0612305](https://arxiv.org/abs/astro-ph/0612305)
- [33] Sun, F., Egami, E., Pirzkal, N., Rieke, M., Baum, S., Boyer, M., Boyett, K., Bunker, A.J., Cameron, A.J., Curti, M., Eisenstein, D.J., Gennaro, M., Greene, T.P., Jaffe, D., Kelly, D., Koekemoer, A.M., Kumari, N., Maiolino, R., Maseda, M., Perna, M., Rest, A., Robertson, B.E., Schlawin, E., Smit, R., Stansberry, J., Sunnquist, B., Tacchella, S., Williams, C.C., Willmer, C.N.A.: First Sample of $H\alpha + [O\ III]\lambda 5007$ Line Emitters at $z \lesssim 6$ Through JWST/NIRCam Slitless Spectroscopy: Physical Properties and Line-luminosity Functions. *ApJ* **953**(1), 53 (2023) <https://doi.org/10.3847/1538-4357/acd53c> [arXiv:2209.03374](https://arxiv.org/abs/2209.03374) [astro-ph.GA]
- [34] Sanders, R.L., Shapley, A.E., Topping, M.W., Reddy, N.A., Brammer, G.B.: Excitation and Ionization Properties of Star-forming Galaxies at $z=2.0-9.3$ with JWST/NIRSpec. *arXiv e-prints*, 2301–06696 (2023) <https://doi.org/10.48550/arXiv.2301.06696> [arXiv:2301.06696](https://arxiv.org/abs/2301.06696) [astro-ph.GA]
- [35] Nakajima, K., Ouchi, M., Isobe, Y., Harikane, Y., Zhang, Y., Ono, Y., Umeda, H., Oguri, M.: JWST Census for the Mass-Metallicity Star-Formation Relations

at $z=4-10$ with the Self-Consistent Flux Calibration and the Proper Metallicity Calibrators. arXiv e-prints, 2301–12825 (2023) <https://doi.org/10.48550/arXiv.2301.12825> arXiv:2301.12825 [astro-ph.GA]

- [36] Keel, W.C., Chojnowski, S.D., Bennert, V.N., Schawinski, K., Lintott, C.J., Lynn, S., Pancoast, A., Harris, C., Nierenberg, A.M., Sonnenfeld, A., Proctor, R.: The Galaxy Zoo survey for giant AGN-ionized clouds: past and present black hole accretion events. *MNRAS* **420**(1), 878–900 (2012) <https://doi.org/10.1111/j.1365-2966.2011.20101.x> arXiv:1110.6921 [astro-ph.CO]
- [37] Maiolino, R., Scholtz, J., Curtis-Lake, E., Carniani, S., Baker, W., de Graaff, A., Tacchella, S., Übler, H., D’Eugenio, F., Witstok, J., Curti, M., Arribas, S., Bunker, A.J., Charlot, S., Chevallard, J., Eisenstein, D.J., Egami, E., Ji, Z., Jones, G.C., Lyu, J., Rawle, T., Robertson, B., Rujopakarn, W., Perna, M., Sun, F., Venturi, G., Williams, C.C., Willott, C.: JADES. The diverse population of infant Black Holes at $4 < z < 11$: merging, tiny, poor, but mighty. arXiv e-prints, 2308–01230 (2023) <https://doi.org/10.48550/arXiv.2308.01230> arXiv:2308.01230 [astro-ph.GA]
- [38] Van Wassenhove, S., Volonteri, M., Mayer, L., Dotti, M., Bellovary, J., Calligaris, S.: Observability of Dual Active Galactic Nuclei in Merging Galaxies. *ApJ* **748**(1), 7 (2012) <https://doi.org/10.1088/2041-8205/748/1/L7> arXiv:1111.0223 [astro-ph.CO]
- [39] Agazie, G., Anumarlapudi, A., Archibald, A.M., Baker, P.T., Bécsy, B., Blecha, L., Bonilla, A., Brazier, A., Brook, P.R., Burke-Spolaor, S., Burnette, R., Case, R., Casey-Clyde, J.A., Charisi, M., Chatterjee, S., Chatziioannou, K., Cheeseboro, B.D., Chen, S., Cohen, T., Cordes, J.M., Cornish, N.J., Crawford, F., Cromartie, H.T., Crowter, K., Cutler, C.J., D’Orazio, D.J., Decesar, M.E., Degan, D., Demorest, P.B., Deng, H., Dolch, T., Drachler, B., Ferrara, E.C., Fiore, W., Fonseca, E., Freedman, G.E., Gardiner, E., Garver-Daniels, N., Gentile, P.A., Gersbach, K.A., Glaser, J., Good, D.C., Gültekin, K., Hazboun, J.S., Hourihane, S., Islo, K., Jennings, R.J., Johnson, A., Jones, M.L., Kaiser, A.R., Kaplan, D.L., Kelley, L.Z., Kerr, M., Key, J.S., Laal, N., Lam, M.T., Lamb, W.G., Lazio, T.J.W., Lewandowska, N., Littenberg, T.B., Liu, T., Luo, J., Lynch, R.S., Ma, C.-P., Madison, D.R., McEwen, A., McKee, J.W., McLaughlin, M.A., McMann, N., Meyers, B.W., Meyers, P.M., Mingarelli, C.M.F., Mitridate, A., Natarajan, P., Ng, C., Nice, D.J., Ocker, S.K., Olum, K.D., Pennucci, T.T., Perera, B.B.P., Petrov, P., Pol, N.S., Radovan, H.A., Ransom, S.M., Ray, P.S., Romano, J.D., Runnoe, J.C., Sardesai, S.C., Schmiedekamp, A., Schmiedekamp, C., Schmitz, K., Schult, L., Shapiro-Albert, B.J., Siemens, X., Simon, J., Siwek, M.S., Stairs, I.H., Stinebring, D.R., Stovall, K., Sun, J.P., Susobhanan, A., Swiggum, J.K., Taylor, J., Taylor, S.R., Turner, J.E., Unal, C., Vallisneri, M., Vigeland, S.J., Wachter, J.M., Wahl, H.M., Wang, Q., Witt, C.A., Wright, D., Young, O., Nanograv Collaboration: The NANOGrav 15 yr Data Set: Constraints on Supermassive Black Hole Binaries from the Gravitational-wave Background. *ApJ* **952**(2), 37 (2023)

<https://doi.org/10.3847/2041-8213/ace18b> arXiv:2306.16220 [astro-ph.HE]

- [40] Kewley, L.J., Dopita, M.A., Sutherland, R.S., Heisler, C.A., Trevena, J.: Theoretical modeling of starburst galaxies. *ApJ* **556**(1), 121–140 (2001) <https://doi.org/10.1086/321545>
- [41] Kauffmann, G., Heckman, T.M., Tremonti, C., Brinchmann, J., Charlot, S., White, S.D.M., Ridgway, S.E., Brinkmann, J., Fukugita, M., Hall, P.B., Ivezić, Ž., Richards, G.T., Schneider, D.P.: The host galaxies of active galactic nuclei. *MNRAS* **346**, 1055–1077 (2003) <https://doi.org/10.1111/j.1365-2966.2003.07154.x>
- [42] Strom, A.L., Steidel, C.C., Rudie, G.C., Trainor, R.F., Pettini, M., Reddy, N.A.: Nebular Emission Line Ratios in $z \approx 2-3$ Star-forming Galaxies with KBSS-MOSFIRE: Exploring the Impact of Ionization, Excitation, and Nitrogen-to-Oxygen Ratio. *ApJ* **836**(2), 164 (2017) <https://doi.org/10.3847/1538-4357/836/2/164> arXiv:1608.02587 [astro-ph.GA]
- [43] Abazajian, K.N., Adelman-McCarthy, J.K., Agüeros, M.A., Allam, S.S., Allende Prieto, C., An, D., Anderson, K.S.J., Anderson, S.F., Annis, J., Bahcall, N.A., Bailer-Jones, C.A.L., Barentine, J.C., Bassett, B.A., Becker, A.C., Beers, T.C., Bell, E.F., Belokurov, V., Berlind, A.A., Berman, E.F., Bernardi, M., Bickerton, S.J., Bizyaev, D., Blakeslee, J.P., Blanton, M.R., Bochanski, J.J., Boroski, W.N., Brewington, H.J., Brinchmann, J., Brinkmann, J., Brunner, R.J., Budavári, T., Carey, L.N., Carliles, S., Carr, M.A., Castander, F.J., Cinabro, D., Connolly, A.J., Csabai, I., Cunha, C.E., Czarapata, P.C., Davenport, J.R.A., de Haas, E., Dilday, B., Doi, M., Eisenstein, D.J., Evans, M.L., Evans, N.W., Fan, X., Friedman, S.D., Frieman, J.A., Fukugita, M., Gänsicke, B.T., Gates, E., Gillespie, B., Gilmore, G., Gonzalez, B., Gonzalez, C.F., Grebel, E.K., Gunn, J.E., Györy, Z., Hall, P.B., Harding, P., Harris, F.H., Harvanek, M., Hawley, S.L., Hayes, J.J.E., Heckman, T.M., Hendry, J.S., Hennessy, G.S., Hindsley, R.B., Hobbitt, J., Hogan, C.J., Hogg, D.W., Holtzman, J.A., Hyde, J.B., Ichikawa, S.-i., Ichikawa, T., Im, M., Ivezić, Ž., Jester, S., Jiang, L., Johnson, J.A., Jorgensen, A.M., Jurić, M., Kent, S.M., Kessler, R., Kleinman, S.J., Knapp, G.R., Konishi, K., Kron, R.G., Krzesinski, J., Kuropatkin, N., Lampeitl, H., Lebedeva, S., Lee, M.G., Lee, Y.S., French Leger, R., Lépine, S., Li, N., Lima, M., Lin, H., Long, D.C., Loomis, C.P., Loveday, J., Lupton, R.H., Magnier, E., Malanushenko, O., Malanushenko, V., Mandelbaum, R., Margon, B., Marriner, J.P., Martínez-Delgado, D., Matsumura, T., McGehee, P.M., McKay, T.A., Meiksin, A., Morrison, H.L., Mullally, F., Munn, J.A., Murphy, T., Nash, T., Nebot, A., Neilsen, J. Eric H., Newberg, H.J., Newman, P.R., Nichol, R.C., Nicinski, T., Nieto-Santisteban, M., Nitta, A., Okamura, S., Oravetz, D.J., Ostriker, J.P., Owen, R., Padmanabhan, N., Pan, K., Park, C., Pauls, G., Peoples, J. John, Percival, W.J., Pier, J.R., Pope, A.C., Pourbaix, D., Price, P.A., Purger, N., Quinn, T., Raddick, M.J., Re Fiorentin, P., Richards, G.T., Richmond, M.W., Riess, A.G., Rix, H.-W., Rockosi, C.M., Sako, M., Schlegel, D.J., Schneider, D.P., Scholz, R.-D., Schreiber, M.R., Schwobe, A.D.,

- Seljak, U., Sesar, B., Sheldon, E., Shimasaku, K., Sibley, V.C., Simmons, A.E., Sivarani, T., Allyn Smith, J., Smith, M.C., Smolčić, V., Snedden, S.A., Stebbins, A., Steinmetz, M., Stoughton, C., Strauss, M.A., SubbaRao, M., Suto, Y., Szalay, A.S., Szapudi, I., Szkody, P., Tanaka, M., Tegmark, M., Teodoro, L.F.A., Thakar, A.R., Tremonti, C.A., Tucker, D.L., Uomoto, A., Vanden Berk, D.E., Vandenberg, J., Vidrih, S., Vogeley, M.S., Voges, W., Vogt, N.P., Wadadekar, Y., Watters, S., Weinberg, D.H., West, A.A., White, S.D.M., Wilhite, B.C., Wonders, A.C., Yanny, B., Yocum, D.R., York, D.G., Zehavi, I., Zibetti, S., Zucker, D.B.: The Seventh Data Release of the Sloan Digital Sky Survey. *ApJS* **182**(2), 543–558 (2009) <https://doi.org/10.1088/0067-0049/182/2/543> arXiv:0812.0649 [astro-ph]
- [44] Leclercq, F., Bacon, R., Wisotzki, L., Mitchell, P., Garel, T., Verhamme, A., Blaizot, J., Hashimoto, T., Herenz, E.C., Conseil, S., Cantalupo, S., Inami, H., Contini, T., Richard, J., Maseda, M., Schaye, J., Marino, R.A., Akhlaghi, M., Brinchmann, J., Carollo, M.: The MUSE Hubble Ultra Deep Field Survey. VIII. Extended Lyman- α haloes around high- z star-forming galaxies. *A&A* **608**, 8 (2017) <https://doi.org/10.1051/0004-6361/201731480> arXiv:1710.10271 [astro-ph.GA]
- [45] Netzer, H.: Bolometric correction factors for active galactic nuclei. *MNRAS* **488**(4), 5185–5191 (2019) <https://doi.org/10.1093/mnras/stz2016> arXiv:1907.09534 [astro-ph.GA]
- [46] Perna, M.: The JWST/NIRSpec GTO programme “The Physics of Galaxy Assembly: IFS observations of high- z galaxies”. *IAU Symposium* **373**, 60–62 (2023) <https://doi.org/10.1017/S174392132200374X>
- [47] D’Eugenio, F., Perez-Gonzalez, P., Maiolino, R., Scholtz, J., Perna, M., Circosta, C., Uebler, H., Arribas, S., Boeker, T., Bunker, A., Carniani, S., Charlot, S., Chevallard, J., Cresci, G., Curtis-Lake, E., Jones, G., Kumari, N., Lamperti, I., Looser, T., Parlanti, E., Rix, H.-W., Robertson, B., Rodriguez Del Pino, B., Tacchella, S., Venturi, G., Willott, C.: A fast-rotator post-starburst galaxy quenched by supermassive black-hole feedback at $z=3$. arXiv e-prints, 2308–06317 (2023) <https://doi.org/10.48550/arXiv.2308.06317> arXiv:2308.06317 [astro-ph.GA]
- [48] Jones, G.C., Uebler, H., Perna, M., Arribas, S., Bunker, A.J., Carniani, S., Charlot, S., Maiolino, R., Rodriguez Del Pino, B., Willott, C., Bowler, R.A.A., Boker, T., Cameron, A.J., Chevallard, J., Cresci, G., Curti, M., D’Eugenio, F., Kumari, N., Saxena, A., Scholtz, J., Venturi, G., Witstok, J.: GA-NIFS: JWST/NIRSpec IFU observations of HFLS3 reveal a dense galaxy group at $z\sim 6.3$. arXiv e-prints, 2308–16620 (2023) <https://doi.org/10.48550/arXiv.2308.16620> arXiv:2308.16620 [astro-ph.GA]
- [49] Parlanti, E., Carniani, S., Übler, H., Venturi, G., D’Eugenio, F., Arribas, S., Bunker, A.J., Charlot, S., Lützgendorf, N., Maiolino, R., Perna, M., Rodríguez Del Pino, B., Willott, C.J., Böker, T., Cameron, A.J., Chevallard, J., Circosta, C.,

- Cresci, G., Jones, G.C., Kumari, N., Lamperti, I., Scholtz, J.: GA-NIFS: Early-stage feedback in a heavily obscured AGN at $z = 4.76$. arXiv e-prints, 2309–05713 (2023) [arXiv:2309.05713](https://arxiv.org/abs/2309.05713) [astro-ph.GA]
- [50] Rodríguez Del Pino, B., Perna, M., Arribas, S., D'Eugenio, F., Lamperti, I., Pérez-González, P.G., Übler, H., Bunker, A., Carniani, S., Charlot, S., Maiolino, R., Willott, C.J., Böker, T., Chevallard, J., Cresci, G., Curti, M., Jones, G.C., Parlanti, E., Scholtz, J., Venturi, G.: GA-NIFS: co-evolution within a highly star-forming galaxy group at $z=3.7$ witnessed by JWST/NIRSpec IFS. arXiv e-prints, 2309–14431 (2023) <https://doi.org/10.48550/arXiv.2309.14431> [arXiv:2309.14431](https://arxiv.org/abs/2309.14431) [astro-ph.GA]
- [51] Schreiber, C., Labbé, I., Glazebrook, K., Bekiaris, G., Papovich, C., Costa, T., Elbaz, D., Kacprzak, G.G., Nanayakkara, T., Oesch, P., Pannella, M., Spitler, L., Straatman, C., Tran, K.-V., Wang, T.: Jekyll & Hyde: quiescence and extreme obscuration in a pair of massive galaxies 1.5 Gyr after the Big Bang. *A&A* **611**, 22 (2018) <https://doi.org/10.1051/0004-6361/201731917> [arXiv:1709.03505](https://arxiv.org/abs/1709.03505) [astro-ph.GA]
- [52] Marchesi, S., Civano, F., Elvis, M., Salvato, M., Brusa, M., Comastri, A., Gilli, R., Hasinger, G., Lanzuisi, G., Miyaji, T., Treister, E., Urry, C.M., Vignali, C., Zamorani, G., Allevato, V., Cappelluti, N., Cardamone, C., Finoguenov, A., Griffiths, R.E., Karim, A., Laigle, C., LaMassa, S.M., Jahnke, K., Ranalli, P., Schawinski, K., Schinnerer, E., Silverman, J.D., Smolcic, V., Suh, H., Trakhtenbrot, B.: THECHANDRA COSMOS LEGACYSURVEY: OPTICAL/IR IDENTIFICATIONS. *ApJ* **817**(1), 34 (2016) <https://doi.org/10.3847/0004-637x/817/1/34>
- [53] Luo, B., Brandt, W.N., Xue, Y.Q., Lehmer, B., Alexander, D.M., Bauer, F.E., Vito, F., Yang, G., Basu-Zych, A.R., Comastri, A., Gilli, R., Gu, Q.-S., Hornschemeier, A.E., Koekemoer, A., Liu, T., Mainieri, V., Paolillo, M., Ranalli, P., Rosati, P., Schneider, D.P., Shemmer, O., Smail, I., Sun, M., Tozzi, P., Vignali, C., Wang, J.-X.: The Chandra Deep Field-South Survey: 7 Ms Source Catalogs. *ApJS* **228**(1), 2 (2017) <https://doi.org/10.3847/1538-4365/228/1/2> [arXiv:1611.03501](https://arxiv.org/abs/1611.03501) [astro-ph.GA]
- [54] Christensen, L., Jakobsen, P., Willott, C., Arribas, S., Bunker, A., Charlot, S., Maiolino, R., Perna, M., Übler, H.: Metal enrichment and evolution in four $z > 6.5$ quasar sightlines observed with JWST/NIRSpec. arXiv e-prints, 2309–06470 (2023) [arXiv:2309.06470](https://arxiv.org/abs/2309.06470) [astro-ph.GA]
- [55] Kocevski, D.D., Onoue, M., Inayoshi, K., Trump, J.R., Arrabal Haro, P., Grazian, A., Dickinson, M., Finkelstein, S.L., Kartaltepe, J.S., Hirschmann, M., Fujimoto, S., Juneau, S., Amorin, R.O., Bagley, M.B., Barro, G., Bell, E.F., Bisigello, L., Calabro, A., Cleri, N.J., Cooper, M.C., Ding, X., Grogan, N.A., Ho, L.C., Inoue, A.K., Jiang, L., Jones, B., Koekemoer, A.M., Li, W., Li, Z., McGrath, E.J.,

- Molina, J., Papovich, C., Perez-Gonzalez, P.G., Pirzkal, N., Wilkins, S.M., Yang, G., Yung, L.Y.A.: Hidden Little Monsters: Spectroscopic Identification of Low-Mass, Broad-Line AGN at $z > 5$ with CEERS. arXiv e-prints, 2302–00012 (2023) <https://doi.org/10.48550/arXiv.2302.00012> arXiv:2302.00012 [astro-ph.GA]
- [56] Tozzi, G., Maiolino, R., Cresci, G., Piotrowska, J.M., Belfiore, F., Curti, M., Mannucci, F., Marconi, A.: Unveiling hidden active nuclei in MaNGA star-forming galaxies with He II $\lambda 4686$ line emission. MNRAS **521**(1), 1264–1276 (2023) <https://doi.org/10.1093/mnras/stad506> arXiv:2302.04282 [astro-ph.GA]
- [57] van Dokkum, P.G.: Cosmic-Ray Rejection by Laplacian Edge Detection. PASP **113**(789), 1420–1427 (2001) <https://doi.org/10.1086/323894> arXiv:astro-ph/0108003 [astro-ph]
- [58] Urrutia, T., Wisotzki, L., Kerutt, J., Schmidt, K.B., Herenz, E.C., Klar, J., Saust, R., Werhahn, M., Diener, C., Caruana, J., Krajnović, D., Bacon, R., Boogaard, L., Brinchmann, J., Enke, H., Maseda, M., Nanayakkara, T., Richard, J., Steinmetz, M., Weilbacher, P.M.: The MUSE-Wide Survey: survey description and first data release. A&A **624**, 141 (2019) <https://doi.org/10.1051/0004-6361/201834656> arXiv:1811.06549 [astro-ph.GA]
- [59] Bacon, R., Conseil, S., Mary, D., Brinchmann, J., Shepherd, M., Akhlaghi, M., Weilbacher, P.M., Piqueras, L., Wisotzki, L., Lagattuta, D., Epinat, B., Guerou, A., Inami, H., Cantalupo, S., Courbot, J.B., Contini, T., Richard, J., Maseda, M., Bouwens, R., Bouché, N., Kollatschny, W., Schaye, J., Marino, R.A., Pello, R., Herenz, C., Guiderdoni, B., Carollo, M.: The MUSE Hubble Ultra Deep Field Survey. I. Survey description, data reduction, and source detection. A&A **608**, 1 (2017) <https://doi.org/10.1051/0004-6361/201730833> arXiv:1710.03002 [astro-ph.GA]
- [60] Cappellari, M.: Improving the full spectrum fitting method: accurate convolution with Gauss-Hermite functions. MNRAS **466**(1), 798–811 (2017) <https://doi.org/10.1093/mnras/stw3020> arXiv:1607.08538 [astro-ph.GA]
- [61] Cresci, G., Mainieri, V., Brusa, M., Marconi, A., Perna, M., Mannucci, F., Piconcelli, E., Maiolino, R., Feruglio, C., Fiore, F., Bongiorno, A., Lanzuisi, G., Merloni, A., Schramm, M., Silverman, J.D., Civano, F.: Blowin’ in the Wind: Both “Negative” and “Positive” Feedback in an Obscured High- z Quasar. ApJ **799**(1), 82 (2015) <https://doi.org/10.1088/0004-637X/799/1/82> arXiv:1411.4208 [astro-ph.GA]
- [62] Kovacevic, J., Popovic, L.C., Dimitrijevic, M.S.: Analysis of optical Fe II emission in a sample of AGN spectra. ApJS **189**(1), 15–36 (2010) <https://doi.org/10.1088/0067-0049/189/1/15> arXiv:1004.2212 [astro-ph.CO]
- [63] Schwarz, U.J.: Mathematical-statistical Description of the Iterative Beam Removing Technique (Method CLEAN). A&A **65**, 345 (1978)

- [64] Cardelli, J.A., Clayton, G.C., Mathis, J.S.: The Relationship between Infrared, Optical, and Ultraviolet Extinction. *ApJ* **345**, 245 (1989) <https://doi.org/10.1086/167900>
- [65] Pérez-González, P.G., Barro, G., Annunziatella, M., Costantin, L., García-Argumánuez, Á., McGrath, E.J., Mérida, R.M., Zavala, J.A., Haro, P.A., Bagley, M.B., Backhaus, B.E., Behroozi, P., Bell, E.F., Bisigello, L., Buat, V., Calabrò, A., Casey, C.M., Cleri, N.J., Coogan, R.T., Cooper, M.C., Cooray, A.R., Dekel, A., Dickinson, M., Elbaz, D., Ferguson, H.C., Finkelstein, S.L., Fontana, A., Franco, M., Gardner, J.P., Giavalisco, M., Gómez-Guijarro, C., Grazian, A., Grogin, N.A., Guo, Y., Huertas-Company, M., Jogee, S., Kartaltepe, J.S., Kewley, L.J., Kirkpatrick, A., Kocevski, D.D., Koekemoer, A.M., Long, A.S., Lotz, J.M., Lucas, R.A., Papovich, C., Pirzkal, N., Ravindranath, S., Somerville, R.S., Tacchella, S., Trump, J.R., Wang, W., Wilkins, S.M., Wuyts, S., Yang, G., Yung, L.Y.A.: CEERS Key Paper. IV. A Triality in the Nature of HST-dark Galaxies. *ApJ* **946**(1), 16 (2023) <https://doi.org/10.3847/2041-8213/acb3a5> arXiv:2211.00045 [astro-ph.GA]
- [66] Weaver, J.R., Kauffmann, O.B., Ilbert, O., McCracken, H.J., Moneti, A., Toft, S., Brammer, G., Shuntov, M., Davidzon, I., Hsieh, B.C., Laigle, C., Anastasiou, A., Jespersen, C.K., Vinther, J., Capak, P., Casey, C.M., McPartland, C.J.R., Milvang-Jensen, B., Mobasher, B., Sanders, D.B., Zalesky, L., Arnouts, S., Aussel, H., Dunlop, J.S., Faisst, A., Franx, M., Furtak, L.J., Fynbo, J.P.U., Gould, K.M.L., Greve, T.R., Gwyn, S., Kartaltepe, J.S., Kashino, D., Koekemoer, A.M., Kokorev, V., Le Fèvre, O., Lilly, S., Masters, D., Magdis, G., Mehta, V., Peng, Y., Riechers, D.A., Salvato, M., Sawicki, M., Scarlata, C., Scoville, N., Shirley, R., Silverman, J.D., Sneppen, A., Smolčić, V., Steinhardt, C., Stern, D., Tanaka, M., Taniguchi, Y., Teplitz, H.I., Vaccari, M., Wang, W.-H., Zamorani, G.: COSMOS2020: A Panchromatic View of the Universe to $z \sim 10$ from Two Complementary Catalogs. *ApJS* **258**(1), 11 (2022) <https://doi.org/10.3847/1538-4365/ac3078> arXiv:2110.13923 [astro-ph.GA]
- [67] Merlin, E., Castellano, M., Santini, P., Cappelletta, G., Boutsia, K., Schreiber, C., Buitrago, F., Fontana, A., Elbaz, D., Dunlop, J., Grazian, A., McLure, R., McLeod, D., Nonino, M., Milvang-Jensen, B., Derriere, S., Hathi, N.P., Pentericci, L., Fortuni, F., Calabrò, A.: The ASTRODEEP-GS43 catalogue: New photometry and redshifts for the CANDELS GOODS-South field. *A&A* **649**, 22 (2021) <https://doi.org/10.1051/0004-6361/202140310> arXiv:2103.09246 [astro-ph.GA]
- [68] Jin, S., Daddi, E., Liu, D., Smolčić, V., Schinnerer, E., Calabrò, A., Gu, Q., Delhaize, J., Delvecchio, I., Gao, Y., Salvato, M., Puglisi, A., Dickinson, M., Bertoldi, F., Sargent, M., Novak, M., Magdis, G., Aretxaga, I., Wilson, G.W., Capak, P.: “Super-deblended” Dust Emission in Galaxies. II. Far-IR to (Sub)millimeter Photometry and High-redshift Galaxy Candidates in the Full COSMOS Field. *ApJ* **864**(1), 56 (2018) <https://doi.org/10.3847/1538-4357/aad4af> arXiv:1807.04697 [astro-ph.GA]

- [69] Shirley, R., Duncan, K., Campos Varillas, M.C., Hurley, P.D., Małek, K., Roehlly, Y., Smith, M.W.L., Aussel, H., Bakx, T., Buat, V., Burgarella, D., Christopher, N., Duivenvoorden, S., Eales, S., Efstathiou, A., González Solares, E.A., Griffin, M., Jarvis, M., Faro, B.L., Marchetti, L., McCheyne, I., Papadopoulos, A., Penner, K., Pons, E., Prescott, M., Rigby, E., Rottgering, H., Saxena, A., Scudler, J., Vaccari, M., Wang, L., Oliver, S.J.: HELP: the Herschel Extragalactic Legacy Project. *MNRAS* **507**(1), 129–155 (2021) <https://doi.org/10.1093/mnras/stab1526> [arXiv:2105.05659](https://arxiv.org/abs/2105.05659) [astro-ph.GA]
- [70] Rieke, M.J., Robertson, B.E., Tacchella, S., Hainline, K., Johnson, B.D., Hausan, R., Ji, Z., Willmer, C.N.A., Eisenstein, D.J., Puskàs, D., Alberts, S., Arribas, S., Baker, W.M., Baum, S., Bhatawdekar, R., Bonaventura, N., Boyett, K., Bunker, A., Cameron, A.J., Carniani, S., Charlot, S., Chevallard, J., Chen, Z., Curti, M., Curtis-Lake, E., Danhaive, A.L., DeCoursey, C., Dressler, A., Egami, E., Endsley, R., Helton, J.M., Hviding, R.E., Kumari, N., Looser, T., Lyu, J., Maiolino, R., Maseda, M.V., Nelson, E.J., Rieke, G., Rix, H.-W., Sandles, L., Saxena, A., Sharpe, K., Shivaie, I., Skarbinski, M., Smit, R., Stark, D.P., Stone, M., Suess, K.A., Sun, F., Topping, M., Uebler, H., Villanueva, N.C., Wallace, I.B., Williams, C.C., Willott, C., Whitler, L., Witstok, J., Woodrum, C.: JADES Initial Data Release for the Hubble Ultra Deep Field: Revealing the Faint Infrared Sky with Deep JWST NIRCIm Imaging. *arXiv e-prints*, 2306–02466 (2023) <https://doi.org/10.48550/arXiv.2306.02466> [arXiv:2306.02466](https://arxiv.org/abs/2306.02466) [astro-ph.GA]
- [71] Boquien, M., Burgarella, D., Roehlly, Y., Buat, V., Ciesla, L., Corre, D., Inoue, A.K., Salas, H.: CIGALE: a python Code Investigating GALaxy Emission. *A&A* **622**, 103 (2019) <https://doi.org/10.1051/0004-6361/201834156> [arXiv:1811.03094](https://arxiv.org/abs/1811.03094) [astro-ph.GA]
- [72] Circosta, C., Mainieri, V., Padovani, P., Lanzuisi, G., Salvato, M., Harrison, C.M., Kakkad, D., Puglisi, A., Vietri, G., Zamorani, G., Cicone, C., Husemann, B., Vignali, C., Balmaverde, B., Bischetti, M., Bongiorno, A., Brusa, M., Carniani, S., Civano, F., Comastri, A., Cresci, G., Feruglio, C., Fiore, F., Fotopoulou, S., Karim, A., Lamastra, A., Magnelli, B., Mannucci, F., Marconi, A., Merloni, A., Netzer, H., Perna, M., Piconcelli, E., Rodighiero, G., Schinnerer, E., Schramm, M., Schulze, A., Silverman, J., Zappacosta, L.: SUPER. I. Toward an unbiased study of ionized outflows in $z \sim 2$ active galactic nuclei: survey overview and sample characterization. *A&A* **620**, 82 (2018) <https://doi.org/10.1051/0004-6361/201833520> [arXiv:1809.04858](https://arxiv.org/abs/1809.04858) [astro-ph.GA]
- [73] Circosta, C., Mainieri, V., Lamperti, I., Padovani, P., Bischetti, M., Harrison, C.M., Kakkad, D., Zanella, A., Vietri, G., Lanzuisi, G., Salvato, M., Brusa, M., Carniani, S., Cicone, C., Cresci, G., Feruglio, C., Husemann, B., Mannucci, F., Marconi, A., Perna, M., Piconcelli, E., Puglisi, A., Saintonge, A., Schramm, M., Vignali, C., Zappacosta, L.: SUPER. IV. CO(J = 3-2) properties of active galactic nucleus hosts at cosmic noon revealed by ALMA. *A&A* **646**, 96 (2021) <https://doi.org/10.1051/0004-6361/202039270> [arXiv:2012.07965](https://arxiv.org/abs/2012.07965) [astro-ph.GA]

- [74] Kormendy, J., Ho, L.C.: Coevolution (or not) of supermassive black holes and host galaxies. *ARA&A* **51**(1), 511–653 (2013) <https://doi.org/10.1146/annurev-astro-082708-101811>
- [75] Liu, D., Lang, P., Magnelli, B., Schinnerer, E., Leslie, S., Fudamoto, Y., Bondi, M., Groves, B., Jiménez-Andrade, E., Harrington, K., Karim, A., Oesch, P.A., Sargent, M., Vardoulaki, E., Bădescu, T., Moser, L., Bertoldi, F., Battisti, A., da Cunha, E., Zavala, J., Vaccari, M., Davidzon, I., Riechers, D., Aravena, M.: Automated Mining of the ALMA Archive in the COSMOS Field (A³COSMOS). I. Robust ALMA Continuum Photometry Catalogs and Stellar Mass and Star Formation Properties for ~ 700 Galaxies at $z = 0.5-6$. *ApJS* **244**(2), 40 (2019) <https://doi.org/10.3847/1538-4365/ab42da> [arXiv:1910.12872](https://arxiv.org/abs/1910.12872) [astro-ph.GA]
- [76] Donevski, D., Lapi, A., Małek, K., Liu, D., Gómez-Guijarro, C., Davé, R., Kraljic, K., Pantoni, L., Man, A., Fujimoto, S., Feltre, A., Pearson, W., Li, Q., Narayanan, D.: In pursuit of giants. I. The evolution of the dust-to-stellar mass ratio in distant dusty galaxies. *A&A* **644**, 144 (2020) <https://doi.org/10.1051/0004-6361/202038405> [arXiv:2008.09995](https://arxiv.org/abs/2008.09995) [astro-ph.GA]
- [77] Keel, W.C., Bennert, V.N., Pancoast, A., Harris, C.E., Nierenberg, A., Chojnowski, S.D., Moiseev, A.V., Oparin, D.V., Lintott, C.J., Schawinski, K., Mitchell, G., Cornen, C.: AGN photoionization of gas in companion galaxies as a probe of AGN radiation in time and direction. *MNRAS* **483**(4), 4847–4865 (2019) <https://doi.org/10.1093/mnras/sty3332> [arXiv:1711.09936](https://arxiv.org/abs/1711.09936) [astro-ph.GA]
- [78] Perna, M., Arribas, S., Catalán-Torrecilla, C., Colina, L., Bellocchi, E., Fluetsch, A., Maiolino, R., Cazzoli, S., Hernán Caballero, A., Pereira Santaella, M., Piqueras López, J., Rodríguez del Pino, B.: MUSE view of Arp220: Kpc-scale multi-phase outflow and evidence for positive feedback. *A&A* **643**, 139 (2020) <https://doi.org/10.1051/0004-6361/202038328> [arXiv:2009.03353](https://arxiv.org/abs/2009.03353) [astro-ph.GA]
- [79] Sutherland, R.S., Dopita, M.A.: Effects of Preionization in Radiative Shocks. I. Self-consistent Models. *ApJS* **229**(2), 34 (2017) <https://doi.org/10.3847/1538-4365/aa6541> [arXiv:1702.07453](https://arxiv.org/abs/1702.07453) [astro-ph.IM]
- [80] Dalla Bontà, E., Peterson, B.M., Bentz, M.C., Brandt, W.N., Ciroi, S., De Rosa, G., Fonseca Alvarez, G., Grier, C.J., Hall, P.B., Hernández Santisteban, J.V., Ho, L.C., Homayouni, Y., Horne, K., Kochanek, C.S., Li, J.I.-H., Morelli, L., Pizzella, A., Pogge, R.W., Schneider, D.P., Shen, Y., Trump, J.R., Vestergaard, M.: The Sloan Digital Sky Survey Reverberation Mapping Project: Estimating Masses of Black Holes in Quasars with Single-epoch Spectroscopy. *ApJ* **903**(2), 112 (2020) <https://doi.org/10.3847/1538-4357/abbc1c> [arXiv:2007.02963](https://arxiv.org/abs/2007.02963) [astro-ph.GA]
- [81] Cicone, C., Maiolino, R., Marconi, A.: Outflows and complex stellar kinematics in SDSS star-forming galaxies. *A&A* **588**, 41 (2016) <https://doi.org/10.1051/0004-6361/201424514> [arXiv:1601.04715](https://arxiv.org/abs/1601.04715) [astro-ph.GA]

- [82] Villar Martín, M., Perna, M., Humphrey, A., Castro Rodríguez, N., Binette, L., Pérez González, P.G., Mateos, S., Cabrera Lavers, A.: Peculiar emission line spectra of core extremely red BOSS quasars at $z \sim 2-3$: orientation and/or evolution? *A&A* **634**, 116 (2020) <https://doi.org/10.1051/0004-6361/201937086> [arXiv:2001.03379](https://arxiv.org/abs/2001.03379) [astro-ph.GA]
- [83] Elvis, M., Civano, F., Vignali, C., Puccetti, S., Fiore, F., Cappelluti, N., Aldcroft, T.L., Fruscione, A., Zamorani, G., Comastri, A., Brusa, M., Gilli, R., Miyaji, T., Damiani, F., Koekemoer, A.M., Finoguenov, A., Brunner, H., Urry, C.M., Silverman, J., Mainieri, V., Hasinger, G., Griffiths, R., Carollo, M., Hao, H., Guzzo, L., Blain, A., Calzetti, D., Carilli, C., Capak, P., Etori, S., Fabbiano, G., Impey, C., Lilly, S., Mobasher, B., Rich, M., Salvato, M., Sanders, D.B., Schinnerer, E., Scoville, N., Shopbell, P., Taylor, J.E., Taniguchi, Y., Volonteri, M.: The Chandra COSMOS Survey. I. Overview and Point Source Catalog. *ApJS* **184**, 158–171 (2009) <https://doi.org/10.1088/0067-0049/184/1/158> [arXiv:0903.2062](https://arxiv.org/abs/0903.2062)
- [84] Civano, F., Marchesi, S., Comastri, A., Urry, M.C., Elvis, M., Cappelluti, N., Puccetti, S., Brusa, M., Zamorani, G., Hasinger, G., Aldcroft, T., Alexander, D.M., Alleinato, V., Brunner, H., Capak, P., Finoguenov, A., Fiore, F., Fruscione, A., Gilli, R., Glotfelty, K., Griffiths, R.E., Hao, H., Harrison, F.A., Jahnke, K., Kartaltepe, J., Karim, A., LaMassa, S.M., Lanzuisi, G., Miyaji, T., Ranalli, P., Salvato, M., Sargent, M., Scoville, N.J., Schawinski, K., Schinnerer, E., Silverman, J., Smolcic, V., Stern, D., Toft, S., Trakhtenbrot, B., Treister, E., Vignali, C.: The Chandra Cosmos Legacy Survey: Overview and Point Source Catalog. *ApJ* **819**(1), 62 (2016) <https://doi.org/10.3847/0004-637X/819/1/62> [arXiv:1601.00941](https://arxiv.org/abs/1601.00941) [astro-ph.GA]
- [85] Davis, J.E., Bautz, M.W., Dewey, D., Heilmann, R.K., Houck, J.C., Huenemoerder, D.P., Marshall, H.L., Nowak, M.A., Schattner, M.L., Schulz, N.S., Smith, R.K.: Raytracing with MARX: x-ray observatory design, calibration, and support. In: Takahashi, T., Murray, S.S., den Herder, J.-W.A. (eds.) *Space Telescopes and Instrumentation 2012: Ultraviolet to Gamma Ray*. Society of Photo-Optical Instrumentation Engineers (SPIE) Conference Series, vol. 8443, p. 84431 (2012). <https://doi.org/10.1117/12.926937>
- [86] Fruscione, A., McDowell, J.C., Allen, G.E., Brickhouse, N.S., Burke, D.J., Davis, J.E., Durham, N., Elvis, M., Galle, E.C., Harris, D.E., Huenemoerder, D.P., Houck, J.C., Ishibashi, B., Karovska, M., Nicastro, F., Noble, M.S., Nowak, M.A., Primini, F.A., Siemiginowska, A., Smith, R.K., Wise, M.: CIAO: Chandra’s data analysis system. In: Silva, D.R., Doxsey, R.E. (eds.) *Society of Photo-Optical Instrumentation Engineers (SPIE) Conference Series*. Society of Photo-Optical Instrumentation Engineers (SPIE) Conference Series, vol. 6270, p. 62701 (2006). <https://doi.org/10.1117/12.671760>
- [87] Burke, D., Laurino, O., wmcclaugh, Marie-Terrell, dtnguyen2, Günther, H.M., Siemiginowska, A., Budynkiewicz, J., Cheer, H., Aldcroft, T., Deil, C., Sipőcz,

- B., Buchner, J., Donath, A., Laginja, I., Leinweber, K., nplee, Todd: Sherpa/sherpa: Sherpa 4.15.1. <https://doi.org/10.5281/zenodo.7948720> . <https://doi.org/10.5281/zenodo.7948720>
- [88] Mineo, S., Gilfanov, M., Lehmer, B.D., Morrison, G.E., Sunyaev, R.: X-ray emission from star-forming galaxies - III. Calibration of the L_X -SFR relation up to redshift $z \approx 1.3$. MNRAS **437**(2), 1698–1707 (2014) <https://doi.org/10.1093/mnras/stt1999> arXiv:1207.2157 [astro-ph.HE]
- [89] Yang, G., Boquien, M., Buat, V., Burgarella, D., Ciesla, L., Duras, F., Stalevski, M., Brandt, W.N., Papovich, C.: X-CIGALE: Fitting AGN/galaxy SEDs from X-ray to infrared. MNRAS **491**(1), 740–757 (2020) <https://doi.org/10.1093/mnras/stz3001> arXiv:2001.08263 [astro-ph.GA]
- [90] Liu, T., Tozzi, P., Wang, J.-X., Brandt, W.N., Vignali, C., Xue, Y., Schneider, D.P., Comastri, A., Yang, G., Bauer, F.E., Paolillo, M., Luo, B., Gilli, R., Wang, Q.D., Giavalisco, M., Ji, Z., Alexander, D.M., Mainieri, V., Shemmer, O., Koekoer, A., Risaliti, G.: X-Ray Spectral Analyses of AGNs from the 7Ms Chandra Deep Field-South Survey: The Distribution, Variability, and Evolutions of AGN Obscuration. ApJS **232**(1), 8 (2017) <https://doi.org/10.3847/1538-4365/aa7847> arXiv:1703.00657 [astro-ph.GA]
- [91] Herenz, E.C., Wisotzki, L., Saust, R., Kerutt, J., Urrutia, T., Diener, C., Schmidt, K.B., Marino, R.A., de la Vieuville, G., Boogaard, L., Schaye, J., Guiderdoni, B., Richard, J., Bacon, R.: The MUSE-Wide Survey: A determination of the Lyman α emitter luminosity function at $3 \leq z \leq 6$. A&A **621**, 107 (2019) <https://doi.org/10.1051/0004-6361/201834164> arXiv:1810.05037 [astro-ph.GA]
- [92] Schmidt, K.B., Kerutt, J., Wisotzki, L., Urrutia, T., Feltre, A., Maseda, M.V., Nanayakkara, T., Bacon, R., Boogaard, L.A., Conseil, S., Contini, T., Herenz, E.C., Kollatschny, W., Krumpe, M., Leclercq, F., Mahler, G., Matthee, J., Mauerhofer, V., Richard, J., Schaye, J.: Recovery and analysis of rest-frame UV emission lines in 2052 galaxies observed with MUSE at $1.5 \leq z \leq 6.4$. A&A **654**, 80 (2021) <https://doi.org/10.1051/0004-6361/202140876> arXiv:2108.01713 [astro-ph.GA]
- [93] Simpson, J.M., Smail, I., Wang, W.-H., Riechers, D., Dunlop, J.S., Ao, Y., Bourne, N., Bunker, A., Chapman, S.C., Chen, C.-C., Dannerbauer, H., Geach, J.E., Goto, T., Harrison, C.M., Hwang, H.S., Ivison, R.J., Kodama, T., Lee, C.-H., Lee, H.-M., Lee, M., Lim, C.-F., Michałowski, M.J., Rosario, D.J., Shim, H., Shu, X.W., Swinbank, A.M., Tee, W.-L., Toba, Y., Valiante, E., Wang, J., Zheng, X.Z.: An Imperfectly Passive Nature: Bright Submillimeter Emission from Dust-obscured Star Formation in the $z = 3.717$ “Passive” System, ZF 20115. ApJ **844**(1), 10 (2017) <https://doi.org/10.3847/2041-8213/aa7cf2> arXiv:1704.03868 [astro-ph.GA]